# PARAMETER ESTIMATION OF FREQUENCY MODULATED CONTINUOUS WAVE (FMCW) RADAR SIGNAL USING WIGNER-VILLE DISTRIBUTION AND RADON TRANSFORM

*A dissertation submitted in partial fulfillment of the*

*requirement for the award of degree of*

**MASTER of ENGINEERING**

*in*

**ELECTRONICS AND COMMUNICATION ENGINEERING**

*Submitted by*

**Sudhir Kumar**

**Roll No. 801261024**

*Under Supervision of*

**Dr. Sanjay Kumar**

**(Assistant Professor)**

**DEPARTMENT OF ELECTRONICS & COMMUNICATION ENGINEERING**

**THAPAR UNIVERSITY**

(Established under the section 3 of UGC Act, 1956)

**PATIALA-147004 (PUNJAB)**

**JULY, 2014**

# DECLARATION

I hereby declare that the work, which is being presented in the dissertation, entitled "**Parameter Estimation of frequency Modulated Continuous Wave (FM-CW) Radar Signal using Wigner-Ville Distribution and Radon Transform**" in partial fulfillment of the requirements for the award of degree of Master of Engineering in Electronics and Communication Engineering submitted at the Department of Electronics and Communication Engineering of Thapar University, Patiala, is an authentic record of my own work carried out under the guidance of **Dr. Sanjay Kumar (Assistant Professor)**, Department of Electronics and Communication Engineering and refers other research's work which are duly listed in reference section.

The matter presented in this dissertation has not been submitted in any other University/Institute for the award of degree.

**Date:** 15-7-2014

**Sudhir Kumar**
**Roll No. 801261024**

It is certified that the above statement made by the student is correct to the best of my knowledge and belief.

**Date:** 15-7-2014

**Dr. Sanjay Kumar**
**Assistant Professor, ECED**
**Thapar University, Patiala**

**Countersigned by:**

**Dr. Sanjay Sharma**
**Professor and Head, ECED**
**Thapar University, Patiala**

**Dr. S.K. Mohapatra**
**Dean, Academic Affairs**
**Thapar University, Patiala**

# ACKNOWLEDGEMENT

I wish to express my deepest gratitude to **Dr. Sanjay Kumar**, Assistant Professor, ECED, Thapar University, Patiala for his sincere and invaluable guidance, suggestions and constant encouragement, and belief in me, which inspired me to submit my dissertation. I am truly very fortunate to have the opportunity to work with him. He has provided me help in technical writing and presentation style, and I found this guidance to be extremely valuable.

I am also thankful to our **Head of the Department, Prof. (Dr.) Sanjay Sharma** as well as **PG Coordinator, Dr. Kulbir Singh, Associate Professor,** Electronics and Communication Engineering Department. I would like to thank entire faculty and staff of Electronics and Communication Engineering Department.

I take this opportunity to gratefully remember all my family members whose inspirations are always like a light house. The love, affection and immense support provided me by my parents were constant inspiration to reach this stage in my life. I would like to give full credit to my parents for every achievement I had in my life.

Sudhir Kumar

# ABSTRACT

Feature extraction algorithm for a time-frequency method based on Wigner-Ville Distribution (WVD) is used for detection and parameter estimation of Frequency Modulated Continuous Wave (FMCW) radar signal. The proposed method uses the Pseudo-Wigner-Ville Distribution (PWVD) as a time-frequency detection technique and Radon Transform to identify the parameter of the modulation. Radon Transform is the projection of the image intensity along a radial line oriented at a specific angle it transforms a 2-D image with lines (line-trends) into a domain of the possible line parameters. The Wigner-Ville Radon Transform (WVRT) is suboptimal in detection and parameter estimation of FMCW low probability of intercept (LPI) radar waveform. Autonomously detecting and analyzing of FMCW can eliminate the need of human intervention. The proposed algorithm can extract FMCW radar modulation parameter efficiently.

# TABLE OF CONTENTS

# LIST OF FIGURES

# LIST OF TABLES

# LIST OF SYMBOLS

| | |
|---|---|
| $R_{Rmax}$ | Maximum Range |
| $R_{Imax}$ | Maximum Interception |
| $f_0$ | Initial Frequency |
| $f_1$ | End Frequency |
| $\alpha$ | Rate of Change of Frequency |
| $\tau$ | Time delay |
| $f_T$ | Transmit Signal Frequency |
| $f_R$ | Received Signal Frequency |
| $f_B$ | Beat Frequency |
| $B$ | Bandwidth |
| $T$ | Code Period |
| $f_c$ | Carrier Frequency |
| $\Delta F$ | Modulation Bandwidth |
| $t_m$ | Modulation Period |
| $\Delta R$ | Range Resolution |
| $f_d$ | Doppler Frequency |
| $\omega$ | Angular Frequency |
| $\Delta T_w$ | Time Resolution |
| $\Delta f_w$ | Frequency Resolution |
| $F_s$ | Sampling Frequency |
| $F_c$ | Carrier Frequency |
| $N_c$ | Number of Subcodes |
| $\rho$ | Smallest Distance from the origin |
| $\theta$ | Angle with x-axis |
| $\mathrm{E_R}$ | Relative Error |
| $V_E$ | Extracted Value |
| $\mathrm{V_T}$ | True Value |

# NOMENCLATURE

| | |
|---|---|
| CW | Continuous Wave |
| FM-CW | Frequency Modulated Continuous Wave |
| WVD | Wigner-Ville Distribution |
| STC | Sensitive Time Control |
| TFA | Time Frequency Analysis |
| DFT | Discrete Fourier Transform |
| PWVD | Pseudo Wigner-Ville Distribution |
| LPI | Low Probability of Intercept |
| LPID | Low Probability of Identification Radar |
| CWD | Choi-Williams Distribution |
| QMFB | Quadrature Mirror Filter Bank |
| RT | Radon Transform |
| ES | Electronic Support |
| SNR | Signal to Noise Ratio |

# CHAPTER 1
# INTRODUCTION

## 1.1 OVERVIEW

Autonomous detection and classification of Frequency Modulated Continuous Wave (FM-CW) can eliminate the need for a human operator and enable near real-time coherent handling of the threat emitters being intercepted. Parameter extraction followed by correlation with existing emitters in a database (identification) can then aid in signal tracking and response management [1].

This examines a pattern recognition technique and parameter extraction of FM-CW. The detection technique examined the Time-Frequency (T-F) techniques Wigner-Ville distribution (WVD).

A feature vector is generated by autonomously cropping the modulation energy from T-F images. First a Two-Dimensional Fast-Fourier transform (2-D FFT) of the images is taken and a frequency domain low pass filter is applied to the transformed images. Following the filtering, autonomous signal energy cropping is performed using an adaptive threshold based on the marginal frequency distribution of the filtered images. After signal energy cropping, the feature vectors are generated by resizing the new images and stacking the columns of the images onto each other [1].

For the WVD images, Radon transform is used to extract the waveform parameters. The Radon transform is the projection of the image intensity along a radial line oriented at a specific angle. It transforms the image with time frequency domain into parameter domain [2].

The test results obtained from algorithm tend to coincide well with the actual values and the relative error depends on how closely results are examined. Up to Signal to Noise Ratio ($SNR$) $= -6dB$ the Pseudo Wigner-Ville Distribution (PWVD) parameter extraction algorithm gave reasonable results.

## 1.2 LOW PROBABILITY OF INTERCEPT RADAR

With the development of advanced electronic support (ES) receivers, radar warning receivers and electronic attack systems such as anti-radiation missiles the threat against high power pulsed radar systems has increased. The interception of radar transmissions may lead to significant vulnerability. To be able to survive and operate effectively, the radar systems need to deny signal interception and be invisible. Invisibility is the property of radar which allows it to see but not be seen. These radar systems are said to have low probability of intercept and are called LPI radar systems. Some of these properties are as follows [1, 3, 4]:

- Low side lobe antennas with infrequent scan modulation,
- The use of broad non-scanning transmitting beam combined with a stationary set of receive beams,
- Reducing the radar power when tracking a closing target,
- Reducing peak power while maintaining the required average power,
- Making use of waveform coding to provide transmitting duty cycles approaching to one and using frequency hopping to force the interceptor to consider more of the spectrum to characterize the radar,
- Wideband continuous waveform (CW) emission,
- Atmospheric attenuation shielding at high frequencies,
- Very high receiver sensitivity,
- High processing gain,
- Coherent detection.

These techniques provide the ability for the LPI radar to detect and track targets without being detected by the intercepting receiver system. LPI radars take advantage of a large time-bandwidth product by reducing its transmitted peak power.

Depending on the purpose or mission of the radar, the type of receiver that is trying to detect it and the engagement geometry, three levels of LPI can be defined as follows [1]:

- The radar is easily detectable but not easily identifiable-called a low probability of identification (LPID) radar,

- The radar can detect a target and is not detectable by an ES receiver at the same range but outside its main beam,
- The radar can detect a target and is not detectable by an ES receiver located on the target-a "quiet radar".

The spread spectrum characteristic of LPI radar is related to the waveform design. Pulse compression modulation techniques provide a wideband LPI CW transmit waveform which is spread over a wide frequency range in a manner that is initially unknown to a hostile receiver. The wide bandwidth makes the interception of the signal more difficult. Some of these wideband CW techniques include [1]:

- Linear and Non-Linear frequency modulation,
- Frequency hopping (frequency shift keying FSK), Costas arrays,
- Phase modulation (phase shift keying PSK),
- Combined phase modulation and frequency hopping (PSK/FSK),
- Random signal modulation.

The ratio of range at which the radar signal can be detected by an intercept receiver to the range at which it can detect a target is an example of the performance parameter for LPI radar [1]. This ratio is given as [1, 5]:

$$\alpha = \frac{R_{Imax}}{R_{Rmax}} \tag{1.1}$$

where $R_{Rmax}$ is the maximum range at which the LPI radar can detect a target and $R_{Imax}$ is the maximum interception receiver detection range. If $\alpha < 1$, then the LPI radar can detect the targets at further ranges without being detected by the intercept receiver. If $\alpha = 1$, then the radar cannot be intercepted beyond the range at which it can detect targets. This also determines the maximum detection range of the LPI radar without being detected by the intercept receiver [1].

## 1.3 FREQUENCY MODULATED CONTINUOUS WAVE

FM-CW radar (Frequency Modulated Continuous Wave radar) is a special type of radar which radiates continuous transmission power like simple continuous wave radar. In contrast to this, FM-CW radar can change its operating frequency during the measurement that is the transmission signal is modulated in frequency. Possibilities of

radar measurements through runtime measurements are only technically possible with these changes in the frequency [6].

Simple continuous wave radar devices without frequency modulation have the disadvantage that they can't measure distances due to missing time reference. Such a time reference for measuring the distance of stationary objects, but can be generated using of frequency modulation of the transmitted signal. In this method, a signal is transmitted, which changes periodically in the frequency. When an echo signal is received then change of frequency gets a delay.

## 1.4 CHARACTERISTIC OF FM-CW RADAR

The distance measurement is accomplished by comparing the frequency of the received signal to a reference [1]. The duration of the transmission signal is substantially greater than the required receiving time for the installed distance measuring range.

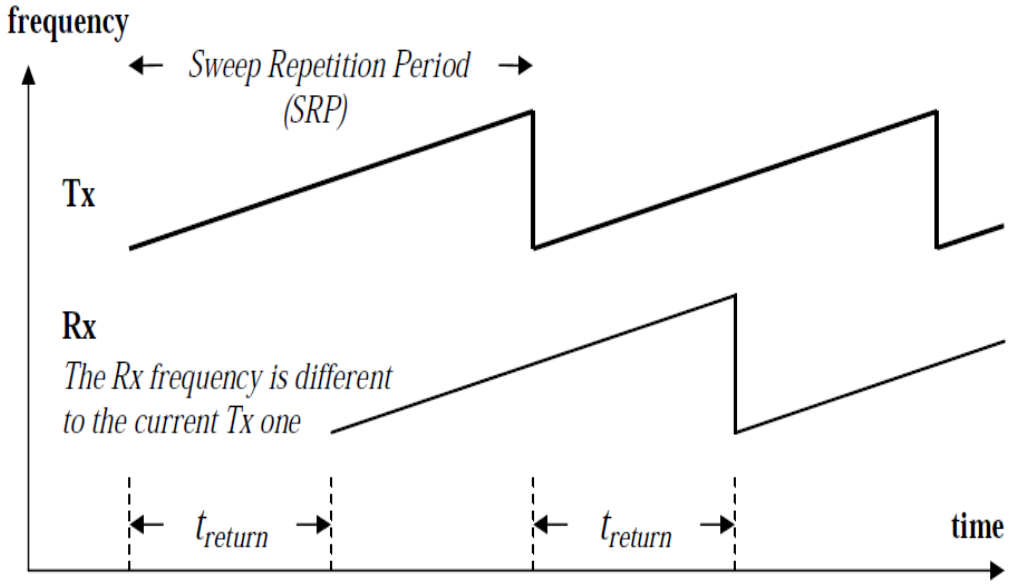


**Figure 1.1: Radar Signal Waveform [3].**

Frequency Modulated Continuous Wave Radar transmits a frequency sweep, often called a chirp. The signal is reflected from distant targets and detected by the receiver where the return signal is mixed with a copy of the transmitted signal to determine the range of the target.

The transmitted waveform has a time varying frequency $f(t)$ given by

$$f(t) = f_0 + \alpha . t \qquad t < T \qquad (1.2)$$

where $f_0$ is the initial frequency, $\alpha$ the Rate of Change of Frequency and $T$ is the Sweep time.

The linearly increasing frequency sweep as shown in Figure 1.2. The frequency is $f_0$ at the start of the sweep and increases to $f_1$ at the end of the sweep after a time $T$ called the sweep period [9]. The bandwidth B is the difference between $f_1$ and $f_0$.

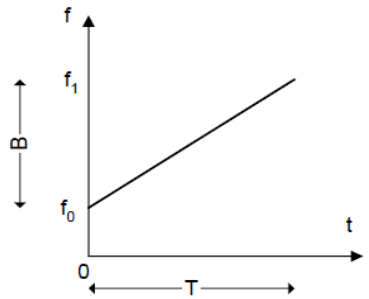


**Figure 1.2: FM-CW Radar Sweep [9].**

The rate of change of frequency is then given by

$$\alpha = \frac{B}{T} \tag{1.3}$$

The phase of the waveform is given by

$$\emptyset(t) = 2\pi \int f(t)\, dt = 2\pi \left( f_0 + \frac{1}{2}\, \alpha\, t^2 \right) \tag{1.4}$$

The transmitted waveform travels to the target at distance $R$ and returns after a time delay $\tau$ given by

$$\tau = \frac{2R}{c} \tag{1.5}$$

where $c$ is the velocity of light in the medium. The process of generating the beat frequency from the return signal can be visualized as shown in Figure 1.3.

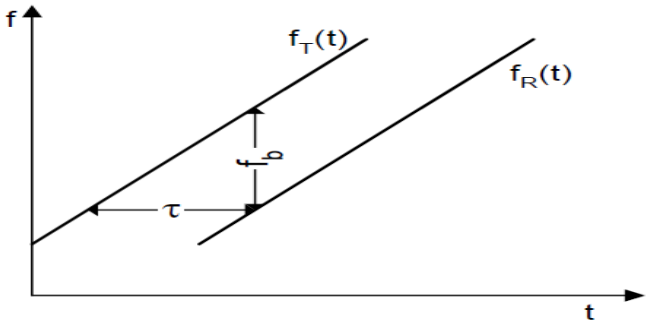


**Figure 1.3: Beat Frequency [9].**

Given that the transmit signal frequency $f_T$ is

$$f_T(t) = f_0 + \alpha.t \qquad\qquad 0 < t \tag{1.6}$$

and assuming an ideal point target, the received signal frequency $f_R$ is given by

$$f_R(t) = f_0 + \alpha.(t - \tau) \qquad \tau < t < T \tag{1.7}$$

Mixing of these two signals produces sum and difference frequencies, $f_T + f_R$and $f_T - f_R$. The resultant signal is then low pass filtered to remove the $f_T + f_R$ term. The term that remains is the beat frequency term $f_B$. The beat frequency term is directly related to the range by Equation 7.

$$\begin{aligned} f_B &= f_T - f_R \\ &= \alpha.t \\ &= \frac{B}{T}.\frac{2R}{c} \\ &= \frac{2RB}{cT} \end{aligned} \tag{1.8}$$

Thus knowing the beat frequency and the radar parameters of *B* and *T*, we can retrieve range information from the return signal.

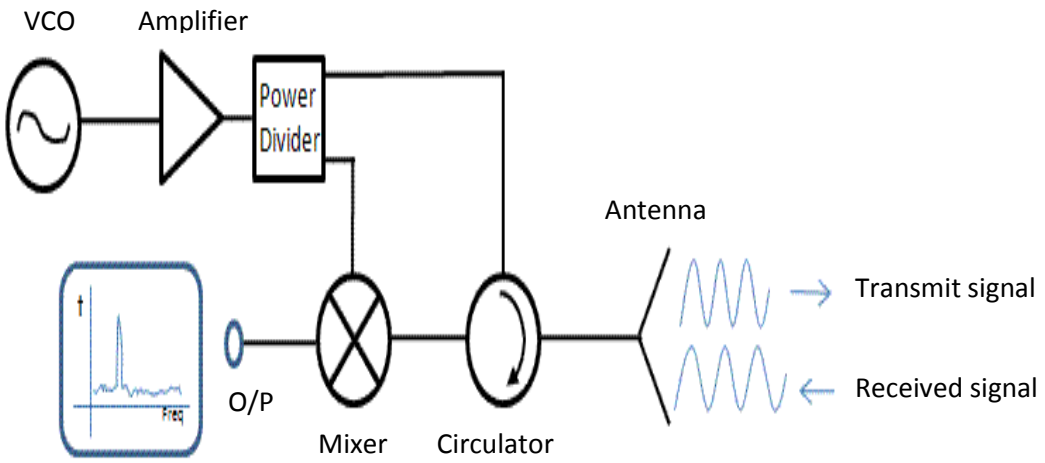


**Figure 1.4: Block diagram of FM-CW radar [10].**

FM-CW signal is the most important and common waveform structure used to achieve low probability of intercept functionality. One of the most important CW modulations utilized is the linear triangular FM-CW emitter, since it can measure the target range and range rate. Some of the properties which make FM-CW waveforms still very effective are as follows [4, 11]:

- Resistance to jamming,
- It is simple to find range information using an FFT,

- Implementation of sensitivity time control (STC) to control dynamic range and prevent saturation in the receiver is easier in the frequency domain,
- The frequency modulation spreads the transmitted energy over a large modulation bandwidth,
- Interception of the emitter's signal is difficult because the power spectrum of the FM-CW signal is nearly rectangular over the modulation bandwidth,
- The transmit waveform is deterministic and the transmit power is low,
- FM-CW modulations are compatible with solid-state transmitters,
- FM-CW is easier to implement than phase code modulation, as long as there is no strict demand on linearity specifications over the modulation bandwidth.

The waveform consists of two linear frequency modulation sections with positive and negative slopes. The frequency of the transmitted waveform for the first section is [1, 4, 12, 13]:

$$f_1 = f_c - \frac{\Delta F}{2} + \frac{\Delta F}{t_m} t \tag{1.9}$$

for $0< t < t_m$ and zero elsewhere. Here $f_c$ is the carrier frequency, $\Delta F$ is modulation bandwidth and $t_m$ is the modulation period, the modulation (sweep) bandwidth $\Delta F$ is chosen to provide the required range resolution

$$\Delta R = \frac{c}{2\Delta F} m \tag{1.10}$$

The frequency of the transmitted waveform for the second section is similarly

$$f_1 = f_c + \frac{\Delta F}{2} - \frac{\Delta F}{t_m} t \tag{1.11}$$

for $0< t < t_m$. The transmit signal for the first section is given by [7, 14, 15, 16]:

$$s_1(t) = a_0 sin\left(2\pi\left(\left(f_c - \frac{\Delta F}{2}\right)t + \frac{\Delta F}{2t_m} t^2\right)\right) \tag{1.12}$$

where $f_c$ is the carrier frequency, $\Delta F$ is modulation bandwidth and $t_m$ is the modulation period, with $0< t < t_m$. The transmit baseband signal for the second section is given by

$$s_2(t) = a_0 sin\left(2\pi\left(\left(f_c + \frac{\Delta F}{2}\right)t - \frac{\Delta F}{2t_m} t^2\right)\right) \tag{1.13}$$

for $t_m < t < 2t_m$. FM-CW signal characteristics are shown in Figure 1.5.

Here $f_{1b}$ and $f_{2b}$ are the beat frequency for the first and second segment respectively, $t_d$ is the round-trip delay time and $f_d$ is the Doppler frequency.

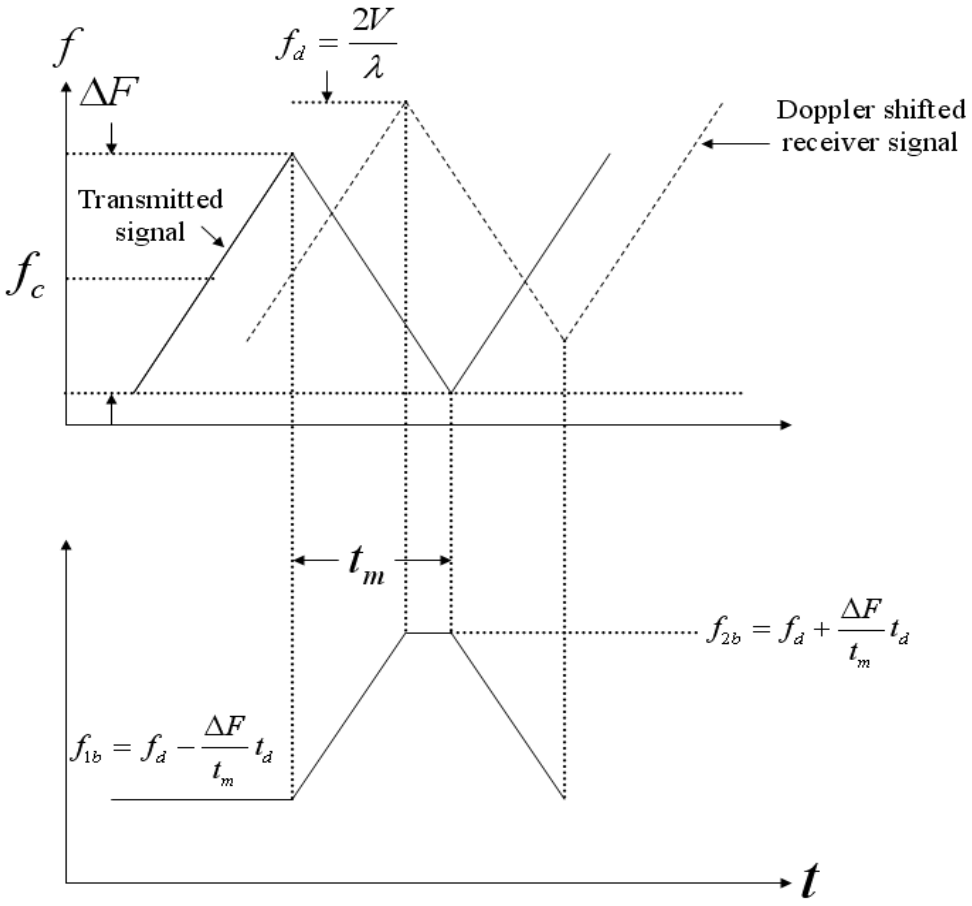


**Figure 1.5: Linear Frequency Modulated Waveform and the Doppler Shifted Return Signal [1].**

## 1.5 WIGNER-VILLE DISTRIBUTION

In many operation radar environments, the non-stationary nature of the received radar signal mandates the use of some form of time-frequency analysis (TFA), which can clearly bring out the non-stationary behavior of the signal. The important virtue of TFA is that it provides an indication of the specific times during which certain spectral components of the signal are observed [1, 6, 7].

Time-frequency analysis allows time and frequency resolution to be controlled independently, but when used for analysis of multi-frequency component signals this approach is vulnerable to cross-terms arising midway between frequency components. There are five techniques, which are in current use. One of them is Wigner Distribution.

Wigner Distribution of a continuous signal x$(t)$ is defined as [14]:

$$WD(t,\omega) = \int_{\tau=-\infty}^{\infty} x\left(t+\frac{\tau}{2}\right).x^*\left(t-\frac{\tau}{2}\right)e^{-i\omega t}d\tau \qquad (1.14)$$

where $t$ is the time variable and $\omega$ is angular frequency $2\pi f$, the integral is from $-\infty\ to\ \infty$, and the * indicates the complex conjugate of the signal $x(t)$. Various formulations of the WD are possible for sampled time series. One of these uses a moving window $w(n)$ with $2N-1$ nonzero values [7].

This continuous time and frequency representation can be modified for the discrete sequence $x(l)$, where $l$ is a discrete time index, $l = \cdots, -1, 0, 1, \ldots$The discrete Wigner distribution $(WD)$ is defined as [14]:

$$WD(l,\omega) = 2\sum_{n=-\infty}^{\infty} x(l+n).x^*(l-n)e^{-j2\omega n} \qquad (1.15)$$

Further modification results in the pseudo-Wigner distribution or windowed-Wigner distribution, which is defined in [6]:

$$WD(l,\omega) = 2\sum_{n=-N}^{N-1} x(l+n).x^*(l-n)w(n)w(-n)e^{-j2\omega n} \qquad (1.16)$$

where $x(l)$ is a discrete input signal with $l$ from $-\infty\ to\ \infty$, $w(n)$ is a length $2N$ real window function with $w(0) = 0$. Here $N$ must be as large as possible within the limits of an acceptable computational cost because a large $N$ gives more output samples, yielding a smoother result [18]. Considering the rectangular window function with a magnitude equal to one the WD becomes [14]:

$$WD(l,\omega) = 2\sum_{n=-N}^{N-1} x(l+n).x^*(l-n)e^{-j2\omega n} \qquad (1.17)$$

Using $f_l(n)$ to represent the kernel function

$$f_l(n) = x(l+n).x^*(l-n) \qquad (1.18)$$

the WD becomes

$$WD(l,\omega) = 2\sum_{n=-N}^{N-1} f_l(n)e^{-j2\omega n} \qquad (1.19)$$

where the continuous frequency variable $\omega$ is sampled by

$$\omega = \frac{\pi k}{2N} \tag{1.20}$$

where $k = 0,1,2,\ldots.2N-1$. The kernel indexes are modified to fit the standard Discrete Fourier Transform$(DFT)$. Since

$$f_l(n) = f_l^*(-n) \tag{1.21}$$

the kernel is a symmetric function, so the Discrete Fourier Transform (DFT) of the kernel is always real.

the WD becomes [14]:

$$WD\left(l, \frac{\pi k}{2N}\right) = 2\sum_{n=-N}^{N-1} f_l(n) exp\left(-\frac{j2\pi nk}{2N}\right) \tag{1.22}$$

Adjusting the limits of *n* in order to use the standard FFT algorithms

$$WD\left(l, \frac{\pi k}{2N}\right) = 2\sum_{n=-N}^{N-1} f_l'(n) exp\left(-\frac{j2\pi kn}{2N}\right) \tag{1.23}$$

Note that the kernel function has been adjusted to $f_l'$ where

$$f_l' = \begin{Bmatrix} f_l(n) & , & 0 \le n \le N-1 \\ 0 & , & n = N \\ f_l(n-2N) & , & N+1 \le n \le 2N-1 \end{Bmatrix} \tag{1.24}$$

The resulting WD is

$$WD(l,\omega) = 2\sum_{n=0}^{2N-1} f_l'(n) e^{-j2\omega n}$$

$$WD(l,\omega) = 2\sum_{n=0}^{2N-1} f_l'(n) exp\left(-\frac{j\pi kn}{N}\right) \tag{1.25}$$

This is the final WD equation.

**Example 1.1**

Suppose there is an input signal [10].

$$x(l) = \{2,4,3,6,1,7\}$$

$$= \{2(l=-3), 4(l=-2), 3(l=-1), 6(l=0), 1(l=1), 7(l=2)\}$$

where the length of the input signal $x(l)$ is $2N = 6$, or $N = 3$. $l$ is a discrete time index from $-N$ to $N-1$. Note that $x = 0$ for $l \leq -4$ or $l \geq 3$ since now $N = 3$, so

$$f_l' = \begin{Bmatrix} f_l(n) & , & 0 \leq n \leq 2 \\ 0 & , & n = 3 \\ f_l(n-6) & , & 4 \leq n \leq 5 \end{Bmatrix}$$

For example, for $l = -3$, the kernel $f'_{-3}(n)$ becomes

$$f'_{-3}(n) = \{f_{-3}(n=0), f_{-3}(n=1), f_{-3}(n=2), f_{-3}(n=3), f_{-3}(n=4), f_{-3}(n=5)\}$$

$$f'_{-3}(n=3) = f_{-3}(n=3) = 0, f'_{-3}(n=0) = f_{-3}(n=4-6) = f_{-3}(n=2)$$

and $f'_{-3}(n=5) = f_{-3}(n=5-6) = f_{-3}(n=-1)$

Hence

$$f'_{-3}(n) = \{f_{-3}(n=0), f_{-3}(n=1), f_{-3}(n=2), 0, f_{-3}(n=-2), f_{-3}(n=-1)\}$$

Recall that $f_l(n) = x(l+n).x^*(l-n)$

$$x(l) = \{2(l=-3), 4(l=-2), 3(l=-1), 6(l=0), 1(l=1), 7(l=2)\}$$

and $x(l) = 0$ for $l \leq -4$ or $l \geq 3$

$f_{-3}(n)$ for input signal $x(l)$ is computed as follows

$$f_{-3}(n=0) = x(-3+0).x^*(-3-0) = x(-3).x^*(-3) = 2.2 = 4$$

$$f_{-3}(n=1) = x(-3+1).x^*(-3-1) = x(-2).x^*(-4) = 4.0 = 0$$

$$f_{-3}(n=2) = x(-3+2).x^*(-3-2) = x(-1).x^*(-5) = 3.0 = 0$$

$$f_{-3}(n=3) = x(-3+3).x^*(-3-3) = x(0).x^*(-6) = 6.0 = 0$$

$$f_{-3}(n=4) = f_{-3}(n=-2) = x(-3-2).x^*(-3+2) = x(-5).x^*(-1) = 0.3 = 0$$

$$f_{-3}(n=5) = f_{-3}(n=-1) = x(-3-1).x^*(-3+1) = x(-4).x^*(-2) = 0.4 = 0$$

So

$$f'_{-3}(n) = \{4,0,0,0,0,0\}$$

and similarly for $l = 0$

$$f_0(n=0) = x(0+0).x^*(0-0) = x(0).x^*(0) = 6.6 = 36$$

$f_0(n=1) = x(0+1).x^*(0-1) = x(1).x^*(-1) = 1.3 = 3$

$f_0(n=2) = x(0+2).x^*(0-2) = x(2).x^*(-2) = 7.4 = 28$

$f_0(n=3) = 0$

$f_0(n=4) = f_0(n=-2) = x(0-2).x^*(0+2) = x(-2).x^*(2) = 4.7 = 28$

$f_0(n=5) = f_0(n=-1) = x(0-1).x^*(0+1) = x(-1).x^*(1) = 3.1 = 3$

Repeating the above procedures, the kernel matrix for $l = -4\ to\ 3$ and $n = 0\ to\ 5$ is as shown in Table 1.

**Table 1: The Kernel $f_l'(n)$ Matrix for the Real Six input [10].**

| | | | | | | |
|---|---|---|---|---|---|---|
| l= 3 | 0 | 0 | 0 | 0 | 0 | 0 |
| l= 2 | 49 | 0 | 0 | 0 | 0 | 0 |
| l= 1 | 1 | 42 | 0 | 0 | 0 | 42 |
| l=0 | 36 | 3 | 28 | 0 | 28 | 3 |
| l= -1 | 9 | 24 | 2 | 0 | 2 | 24 |
| l= -2 | 16 | 6 | 0 | 0 | 0 | 6 |
| l= -3 | 4 | 0 | 0 | 0 | 0 | 0 |
| l= -4 | 0 | 0 | 0 | 0 | 0 | 0 |
| | n=0 | n=1 | n=2 | n=3 | n=4 | n=5 |

The second step is to use to calculate the Wigner distribution. As an example of the calculation, one can pick any *l* and $k$ to examine the values inside the WD matrix.

For example, choose $l = 1, k = 2\ and\ N = 3$. The WD is

$$WD(l=1,k=2) = 2\sum_{n=0}^{2N-1} f_l'(n)exp\left(-\frac{j\pi kn}{N}\right)$$

$$= 2\sum_{n=0}^{2.3-1} f_l'(n)exp\left(-\frac{j\pi 2n}{N}\right)$$

$$= 2\sum_{n=0}^{5} f_l'(n) exp\left(-\frac{j\pi nk}{2N}\right)$$

From the kernel matrix the kernel function for $l = 1$ is

$$f_1'(n) = \{1,42,0,0,0,42\}$$

which means that

$$f_1'(0) = 1, f_1'(1) = 42, f_1'(2) = 0, f_1'(3) = 0, f_1'(4) = 0, f_1'(5) = 42$$

the WD for $l = 1\ and\ k = 2$ is

$$WD(1,2) = 2f_l'(0).exp\left(-\frac{j.\pi.2.0}{3}\right) + 2f_l'(1).exp\left(-\frac{j.\pi.2.1}{3}\right) + 2f_l'(2).exp\left(-\frac{j.\pi.2.2}{3}\right) + 2f_l'(3).exp\left(-\frac{j.\pi.2.3}{3}\right) + 2f_l'(4).exp\left(-\frac{j.\pi.2.4}{3}\right) + 2f_l'(5).exp\left(-\frac{j.\pi.2.5}{3}\right)$$

$$= 2.1.(0) + 2.42.(-0.5000 - 0.8660i) + 2.0 + 2.0 + 2.0 + 2.42.(-0.50000 + 0.8660i)$$

$$= -82$$

Repeating the above procedures, gives the WD matrix at discrete time index $l = -4\ to\ 3$ and discrete frequency index $k = 0\ to\ 5$ .An important feature in this Wigner distribution computation result is that all the components in WD matrix are real.

**Table 1.2: The WD Matrix $WD(l,k)$ for the Real Six input [10].**

| | | | | | | |
|---|---|---|---|---|---|---|
| l= 3 | 0 | 0 | 0 | 0 | 0 | 0 |
| l= 2 | 98 | 98 | 98 | 98 | 98 | 98 |
| l= 1 | 170 | 86 | -82 | -166 | -82 | 86 |
| l=0 | 196 | 22 | 10 | 172 | 10 | 22 |
| l= -1 | 122 | 64 | -34 | -70 | -34 | 62 |
| l= -2 | 56 | 44 | 20 | 8 | 20 | 44 |
| l= -3 | 8 | 8 | 8 | 8 | 8 | 8 |
| l= -4 | 0 | 0 | 0 | 0 | 0 | 0 |
| | k=0 | k=1 | k=2 | k=3 | k=4 | k=5 |

# CHAPTER 2
# LITERATURE REVIEW

Gau *et al.* [1] the parameters of Low Probability of Intercept (LPI) radar signals are hard to identify by using traditional periodogram signal processing techniques. Using the Wigner Distribution (WD), this thesis examines eight types of LPI radar signals. Signal to noise ratios of 0 dB and –6dB are also investigated. The eight types LPI radar signals examined include Frequency Modulation Continuous Wave (FM-CW), Frank code, P1 code, P2 code, P3 code, P4 code, COSTAS frequency hopping and Phase Shift Keying/Frequency Shift Keying (PSK/FSK) signals. Binary Phase Shift Keying (BPSK) signals although not used in modern LPI radars are also examined to further illustrates the principal characteristics of the WD.

Wang *et al.* [3] works on time-frequency tiling based detector for detection of non-linear frequency modulated (NLFM) signal or polynomial phase signal (PPS). The method exploits the time-frequency tiling property of adaptive wavelet transform, and is practically realizable. The unitary and linear phase wavelet basis function together with joint one order linear approaching procedure is presented to estimate the signals trace line in time-frequency plane. the Radon-Wigner (RWT) transform is exploited in subband outputs of time-frequency tiling to achieve low computational complexity implementation.

Gulum *et al.* [6] works on parameter extraction technique for FMCW radar signals using Wigner-Hough-Radon Transform. An autonomous parameter extraction algorithm for frequency modulated continuous wave (FM-CW) radar signals using Wigner-Ville Distribution (WVD) Hough transform was investigated and extraction of poly-phase radar modulation parameters using a Wigner-Ville distribution Radon transform was investigated. Proposed algorithm can extract FM-CW radar modulation parameters at low SNR levels. The results showed that, the algorithm proved well even at low SNR levels. The error between the extracted parameters and the true values were relatively small providing high accuracy rates in average.

Gulum *et al.* [7] works on an autonomous feature extraction algorithm for classification of Low Probability of Intercept (LPI) radar modulations is investigated. A full

investigation of various preprocessing algorithms and classification techniques is applied to a database of important LPI radar waveform modulations including Frequency Modulation Continuous Waveform (FM-CW). These include the Wigner-Ville distribution, the Choi-Williams distribution and quadrature mirror filtering. The Wigner-Ville distribution and the Choi-Williams distribution, two autonomous extraction algorithms are investigated to derive the significant modulation parameters of polyphase coded LPI radar waveform modulations.

Jalil *et al.* [9] works on FM-CW (Frequency Modulated Continuous Wave) radars transmit a continuous frequency modulated wave for target detection. The proposed method describes a method of digital signal processing for extracting and isolating targets in the received signal of FM-CW radar. As opposed to pulsed radar, signal processing of FM-CW is done in frequency domain. The first step in processing is to convert the signal in frequency domain using FFT (Fast Fourier Transform). Digital filtering of the frequency spectrum of the return signal has been done in the MTI (Moving Target Indication) block using Delay Line Canceller. FM-CW Radar data with both targets and clutter was simulated using Matlab, for both sawtooth and triangular waveforms.

Edrich *et al*. [14] works on Ka-Band FM-CW-Radar for sniper detection. The goal is to detect the sniper threat and to estimate the direction and, if possible, the exact location of the threat origin. For an Omni-directional protection around an object or vehicle several sensors are required or an antenna array has to be used. The detection range of the radar is limited the best results in operational conditions will be achieved by performing a sensor fusion with other types of sensors like acoustic ones.

Meta *et al.* [19] work on Signal Processing Algorithms for FM-CW Moving Target Indicator Synthetic Aperture Radar. Analytical development of an FM-CW SAR algorithm starting from the deramped signal and without using the stop-and-go approximation is presented in this paper.

An FM-CW SAR signal description in the two-dimensional frequency domain has been derived without any approximation. From this description an algorithm that corrects for motion within the sweep has been derived and validated by means of simulation and processing of real data.

Wasselin *et al.* [20] works on FM-CW Radar System for Detection and Classification of Small Vessels in High Sea State Conditions. Several test campaigns have been conducted to develop a sensor as well as an innovating signal processing chain which provides the system with a promising capability to detect and classify small vessels in all sea states.

Geroleo *et al.* [21] The Wigner-Ville Hough transform (WVHT) is suboptimal in the detection and parameter estimation of linear frequency-modulated (LFM) continuous wave (LFMCW) low probability of intercept (LPI) radar waveforms because they are composed of concatenated LFM pulses. We formulate the detection and estimation problem to take into account the multiple pulses that are available in an observation interval at the intercept receiver. The new algorithm, called the periodic WVHT (PWVHT), significantly outperforms the WVHT for LFMCW signals.

Hyun *et al.* [22] works on FPGA Based Signal Processing Module Design and Implementation for FM-CW Vehicle Radar System. In this the detection algorithms based on two-step FFT (Fast Fourier Transform) using the several fast ramps in order to resolve radar range-velocity ambiguities. The first FFT, DBF (Digital Beam Forming), The second FFT, and CFAR (Constant False Alarm) onto FPGA.

Toole *et al.* [23] Time-frequency distributions are used in the analysis and processing of non-stationary signals. The Wigner-Ville distribution (WVD) is a fundamental time-frequency distribution uniquely satisfying many desirable mathematical properties. The realization of this distribution for hardware or software platforms requires a discrete version. Historically the majority of the work on deriving discrete versions of the WVD has focused on creating alias-free distributions, often resulting in a loss of some desirable properties. Here a new discrete time and frequency WVD will be presented for non-periodic signals and will be examined both in terms of its properties and aliasing. In particular unitarity, an assumed property for optimum time-frequency detection and signal estimation, and invertibility, a useful property especially for time-frequency filtering, will be examined. An efficient implementation of the distribution using standard real-valued fast Fourier transforms will also be presented.

Spafford *et al.* [24] works on optimum radar signal processing in clutter. When the clutter has a range-time extent less than the equivalent range-time extent of the signal, filter design alone yields nearly optimum performance. In this report it is suggested that the

signal be designed under the assumption of the clutter being extended over a broad range of Doppler and that the signal processor consist of a bank of adaptive filters. Then each filter output yields the maximum ratio of peak signal to total interference power for this signal design.

Carr *et al*. [25] works on digital signal processing for target in FM-CW radar. This type of radar is more difficult to use where there are several targets as detection has to be based on the analysis of the frequency spectrum of the return signal. FM-CW radar was used to detect buried objects the interpretation of the frequency spectrum was performed by visual inspection of the output of a spectrum analyzer. Such a method of interpretation is generally unsatisfactory and describes a method for target extraction using digital-signal-processing techniques.

A number of targets can be extracted from the return of FM-CW radar using a processing technique based on the optimization of a suitable model to the filtered radar return. The optimization algorithm used for detection is capable of extracting targets from clutter and also of separating targets that are so close together that they cannot be separated by eye. Optimization is a complex technique, but it allows the shape information in the spectral return to be used to identify signals hidden by clutter.

Ming *et al*. [26] work on implementation of parallel signal processing system for all-purpose radar. A DSP-based all-purpose radar parallel signal processing system (RPSPS) with high-speed real-time signal processing is implemented to fulfill the all-purpose and system reconfiguration. High performance DSP chips are used as the kernel processing nodes. The system architecture, data distribution and processing of this design are all fit for the characteristic of radar signal.

Chang *et al*. [27] works on practical FM-CW radar signal processing method and its system implementation. This system is mainly used for eliminating noise interference from the sampled signal, checking out the objective signal, and sending the data as the processing results to a computer through the PCI Interfaces. The results are finally processed by the computer and displayed on its screen. The proposed method analyzes the signal processing algorithm, and applies it to the system implementation.

It analyzes how these methods can be applied to engineering projects. This paper introduces a new design scheme of FMCW radar signal processing system. Aimed at the

features of engineer tasks, it divides the tasks (into two parts) using two DSP chips in the concatenation mode. The paper also gives some solutions to the pertinent problems those may occur during the FMCW radar signal processing.

Strobel *et al*. [28] works on a millimeter-wave low power active back scatter tag for FM-CW radar system. In this a fully integrated active backscatter transponder based on the switched injection-locked oscillator (SILO) principle for frequency-modulated continuous-wave radar applications is presented. The SILO backscatter transponder was used to perform distance measurements.

Hu *et al.* [29] works on Design and Realization of High-performance Universal Radar Signal Processing System. The theoretical analysis on the shared bus type and distributed type parallel structure, and according the characteristic of the radar signal processing, one high-performance universal radar signal processing system was designed and realized. The system has the characteristics of standardization, modularization, scalability, restructure, hybrid parallel processing, and multi-layer interconnection.

In practice, using this processing system, matching with corresponding IO module, multiple phased array radar and synthetic aperture radar signal processing system have been structured, and the high-performance and the universality of the system have been validated.

Chongyu *et al.* [30] works on Signal Processing in the Life-Detection Radar Using an FM-CW Waveform. The progresses and difficulties faced in the life detection radar signal processing are introduced in the paper. Echoes from the obstructions in the direction of radar antenna are main interference. How to control the interferences are discussed and a combinative approach of body movement and life information detection is brought forward in the paper.

Significant progresses have been achieved in signal processing, life information abstracting and target recognition. However, because of the complicated detection surroundings, more works are required on suppressing the interference to make the detection technology be more practical.

Barbarossa *et al*. [31] shows that the combined use of the Wigner-Ville Distribution (WVD) and the Hough Transform (HT) provides an important tool for mapping the signals onto a parameter space where the detection and parameter estimation problems

can be made easier. Since the important features of the signal are emphasized. This mapping can be used in the detection and parameter estimation of signals unknown embedded in noise. It is shown that this mapping comes directly from the application of the matched filter theory. In particular, the method can be applied to multi-components signals, since it reduces considerably the effect of the cross terms, produced by the WVD, on the signal parameters estimate.

Li *et al.* [32] proposed a new method based on the Wigner Transformation and Hough Transformation, the new method was used to estimate the number of targets contained in the LFM radar returns. The simulation results show that the number of targets contained in the LFM radar returns can be estimated exactly by this new method. The algorithm is simple and easy to implement in works, so it has good technical expansibility, so it could not only be applied to the field of military, but also the field of civil.

Li *et al.* [33] work on problem of detection polynomial phase signals (PPS) affected by additive Gaussian white noise. A new algorithm for PPS detection is proposed. It is based on the time domain filter-banks method combined with the short time Radon-Wigner transform method. Because of the band-limited character of PPS, the subband signal's signal-to-noise ratio (SNR) can be enhanced by using filter bank method. The local PPS can be approximated by linear frequency modulated (LFM) signal, so short time Radon-Wigner transform is used to detect and estimate the local signal's instantaneous frequency.

Cornelia *et al.* [34] works on Wigner-Ville time-frequency distribution combined with the Hough transform for detection of linear frequency modulated signals. Classical version of the Hough transform to detect linear shape in the frequency representation of the linear FM signals.

Geroleo *et al.* [35] uses the Wigner-Ville Hough transform (WVHT) is suboptimal in the detection and parameter estimation of linear frequency-modulated (LFM) continuous wave (LFMCW) low probability of intercept (LPI) radar waveforms because they are composed of concatenated LFM pulses. The new algorithm, called the periodic WVHT (PWVHT), significantly outperforms the WVHT for LFMCW signals.

Cirillo *et al.* [36] Estimation of phase parameters of mono and multicomponent FM signals, with both good numerical properties and statistical performance proposed. The

proposed approach is based on the Hough transform of the pseudo Wigner-Ville time-frequency distribution (PWVD). It is shown that the numerical properties of the estimator may be improved by varying the PWVD window length. The effect of the window time extent on the statistical performance of the estimator is delineated.

The proposed approach was verified for nonlinear FM signals in the application to experimental radar data, where multicomponent micro-doppler signatures, modelled as sinusoidal FM, were successfully estimated.

Jianhong *et al.* [37] Proposed method put forwards Radon-Wigner transform to detect multiscatter target echoes. This method will result in derivative cross term components beneficial to extended target detection, at the same time SNR for each scattering center echo is equivalent to pulse compression result from matched filtering method. Radon-Wigner transform can converge the signal energy together to be detected, so it is effective processing method.

Hang *et al.* [38] work on DOA estimation based on time-frequency analysis, eliminating cross interference terms is the key to improve DOA estimation performance for the multi-signal sources situation. PWVD is the most commonly used time-frequency analysis tool for suppressing cross interference terms in WVD. However, the cross terms improvement of PWVD is not so ideal and the estimated results are not so reliable. SPWVD can suppress cross terms better, but the time-frequency concentration performance of signal drops largely. RWT (Radon-Wigner Transform) as time-frequency transform tool is very suitable to describe LFM signals. This method can suppress cross terms in the background of multi sources effectively, possess good time-frequency concentration performance, and consequently it can improve the accuracy of DOA estimation much more greatly.

Wood *et al.* [39] works on Radon transform of a time-frequency distribution produces local areas of signal concentration that facilitate interpretation of multicomponent signals. The Radon-Wigner transform can be efficiently implemented with dechirping in the time domain, however, only half of the possible projections through the time-frequency plane can be realized because of aliasing. Discrete-time equations for both time and frequency dechirping are derived, and highlight some practical implementation issues.

# CHAPTER 3
# DETECTION TECHNIQUES

The autonomous detection, classification and parameter extraction system block diagram used in this work is illustrated in Figure 3.1. The system contains T-F (the Wigner-Ville distribution, the Choi-Williams distribution and Quadrature mirror filter bank) detection techniques. The detection techniques provide an image output. The output image from each detection method is preprocessed to form a feature vector. An autonomous image cropping and feature extraction algorithm based on two-dimensional Fast Fourier Transform (2-D FFT) is applied to the T-F images [18].

Later the extracted features are used as input to a non-linear classifier. The output of the classifiers generates a confusion matrix (CM) which shows the detection results. The columns of the CM represent the input vector modulation type while the rows indicate the assignment by the classifier and the sum of all values should be one. The diagonals of the CM indicate the percentage of correct assignments by the network. Once the modulation is classified, the parameters can be extracted using the T-F images.

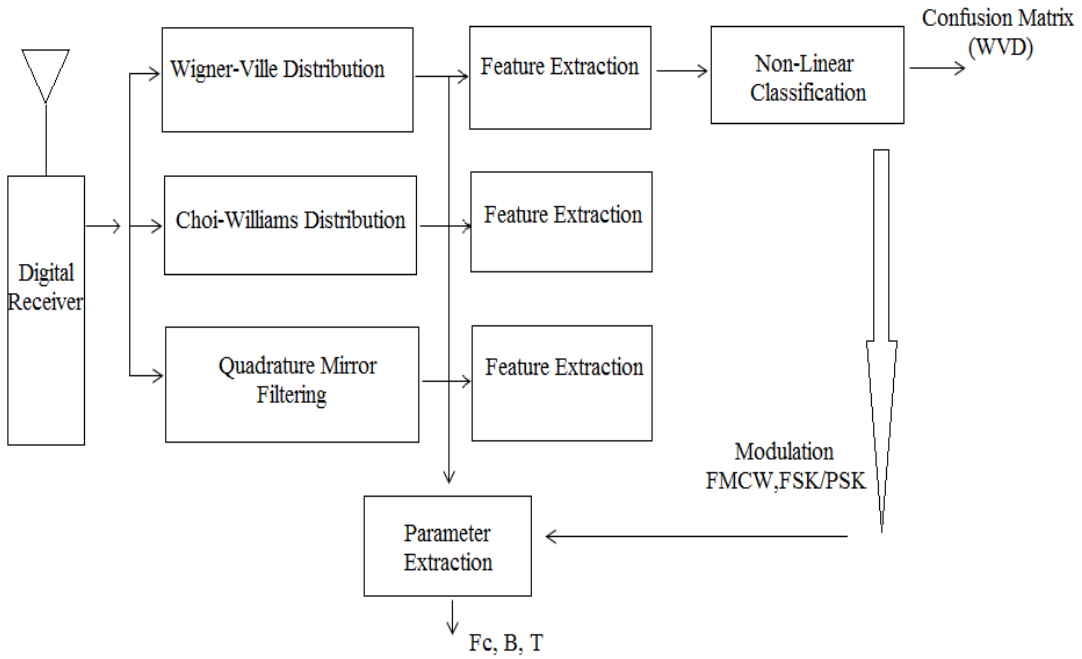


**Figure 3.1: Detection Classification and Parameter Extraction Architecture [18].**

## 3.1 PSEUDO WIGNER-VILLE DISTRIBUTION

One of the most prominent members of T-F energy density functions is the Pseudo Wigner-Ville distribution (WVD). The WVD has been noted as one of the more useful in the Cohen's class of distributions. The PWVD is computed by correlating the signal with time and frequency translated version of itself. The time and frequency marginal properties are preserved for any signal [40]. The PWVD exhibits the highest signal energy concentration in the T-F plane for linearly modulated signals. The PWVD also contains interfering *cross terms* between every pair of signal components which limits its applications. Although several formulations can be used to reduce the amplitude of the cross terms, since the cross terms contain additional T-F information, it is of interest to determine if they facilitate the classification process in comparison to the CWD and QMFB [1].

The WVD of a continuous one-dimensional function $x(t)$ is defined as [1]:

$$W_x(t,\omega) = \int_{-\infty}^{\infty} x\left(t+\frac{\tau}{2}\right) x^*\left(t-\frac{\tau}{2}\right) e^{-i\omega\tau} d\tau \tag{3.1}$$

where $t$ is the time variable, $\omega$ is the angular frequency variable $(2\pi f)$, and the $*$ indicates complex conjugate. Let $x(l)$ be a sampled time series representing the digitized signal where $l$ is a discrete time index from $-\infty$ to $+\infty$. The discrete WVD is:

$$\mathrm{W}(l,\omega) = 2\sum_{-\infty}^{\infty} x(l+n)x^*(l-n)\, e^{-2j\omega n} \tag{3.2}$$

Windowing the data results in the pseudo WVD (PWVD):

$$\mathrm{W}(l,\omega) = 2\sum_{n=-N+1}^{N-1} x(l+n)x^*(l-n)\; w(n)w(-n)e^{-2j\omega n} \tag{3.3}$$

$w(n)$ is a real valued window with length 2N-1 and $w(0) = 1$. Using $f_l(n)$ to represent the kernel function:

$$f_l(n) = x(l+n)x^*(l-n)w(n)w(-n) \tag{3.4}$$

the PWVD becomes:

$$W(l,\omega) = 2\sum_{n=-N+1}^{N-1} f_l(n)e^{-2j\omega n} \tag{3.5}$$

where $\omega = \frac{\pi k}{2N}$ and $k = 0,1,2, \ldots .2N - 1$. The kernel indexes are modified to fit the standard Discrete Fourier Transform$(DFT)$. Since $f_l(n) = f_l^*(-n)$, only $f_l(n)$ needs to be computed for $n \geq 0$ [1].

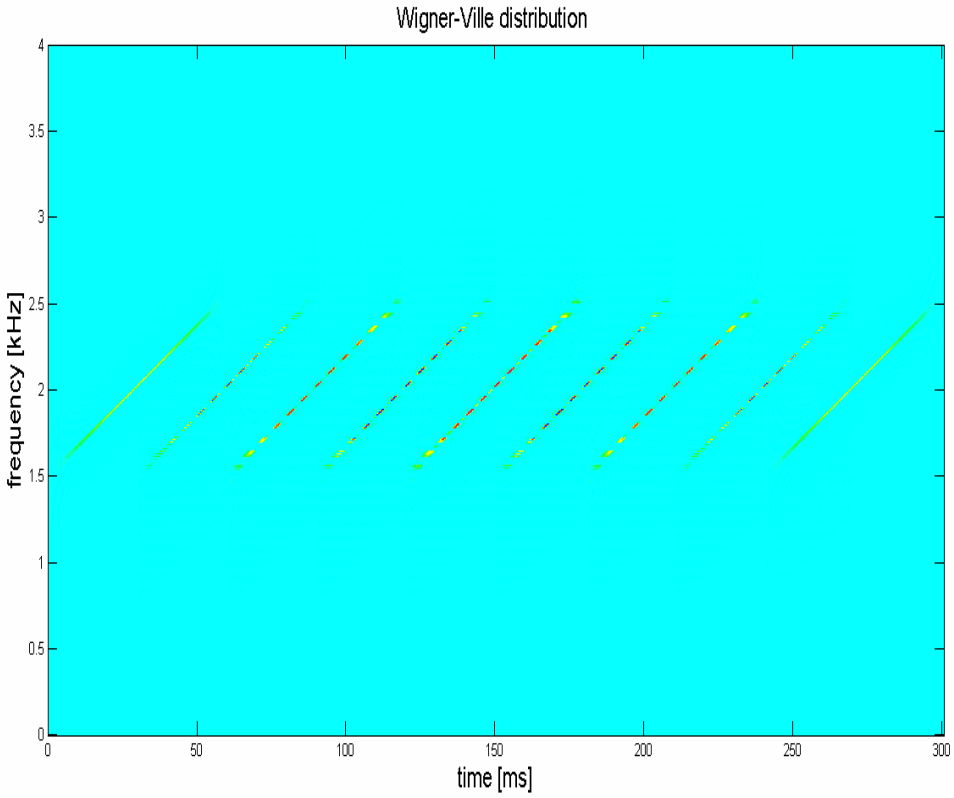


**Figure 3.2: Pseudo Wigner-Ville Distribution of FM-CW Signal.**

Figure 3.2 shows the PWVD results for a FM-CW Signal with a carrier frequency of $F_c = 2000\,Hz$ with a sampling frequency of $F_s = 8KHz$ in a contour plot. With the number of carrier frequency cycles within a sub code of $cpp = 1$. The transmitted bandwidth $B = \frac{F_c}{cpp} = 2000\,Hz$ and the code period is $T = 8.6\,ms$. Note the presence of the characteristic cross terms. Note also that with the PWVD time-frequency information, the signal parameters can be measured accurately including the number of subcodes $N_c = \frac{T}{B}$ . The frequency resolution of the WVD $\Delta f_w = \frac{F_s}{2N}$ and the time resolution $\Delta T_w = \frac{1}{F_s}$ . For efficiency the implementation of the Wigner-Ville distribution used in this work was established by [41].

### 3.2 CHOI-WILLIAMS DISTRIBUTION

The Choi-Williams Distribution (CWD) simultaneously gives the representation of a signal in both time and frequency. The CWD has been noted as one of the more useful in the Cohen's class of distributions since it reduces the amplitude of the cross terms [7]. This distribution is a bilinear time-frequency analysis techniques for signal processing and has been used in many fields of engineering.

The CWD is given as [16]:

$$C_x(t,v;f) = \iiint_{\infty} e^{j2\pi\xi(s-t)} f(\xi,\tau) x\left(s+{}^{\tau}/_{2}\right) x^*\left(s-{}^{\tau}/_{2}\right) e^{-j2\pi v} d\xi ds d\tau \quad (3.6)$$

where $f(\xi,\tau)$a 2-D function is called the *parameterization function*. A natural choice for the kernel is to consider a Gaussian function:

$$f(\xi,\tau) = e^{-(\pi\xi\tau)^2/2\sigma^2} \quad (3.7)$$

resulting in

$$CW_x(t,v) = \sqrt{\frac{2}{\pi}} \iint_{\infty} \frac{\sigma}{|\tau|} e^{-2\sigma^2(s-t)^2/\tau^2} x\left(s+{}^{\tau}/_{2}\right) x^*\left(s-{}^{\tau}/_{2}\right) e^{-j2\pi v\tau} ds d\tau \quad (3.8)$$

The frequency-resolution and the suppression of the cross-terms can be controlled by varying the $\sigma$. The smaller the parameter $\sigma$, the more the cross-terms are suppressed. But this also will affect the auto-terms. Therefore, there is trade-off for the selection of the parameter $\sigma$ [40]. Note that as $\sigma \to \infty$, the corresponding distribution converges to the Wigner-Ville distribution. Note that this means to set the parameterization function to one, $f(\xi,\tau) = 1$.

Figure 3.3 shows the Choi-Williams results for a FM-CW Signal with a carrier frequency of $F_c = 1495\ Hz$ with a sampling frequency of $F_s = 8KHz$ in a contour plot. With the number of carrier frequency cycles within a sub code of $cpp = 1$. The transmitted bandwidth $B = \frac{F_c}{cpp} = 1495\ Hz$ and the code period is $T = 8.6\ ms$. Note that with the CWD time-frequency information, the signal parameters can also be measured accurately including the number of sub codes $N_c = {}^{T}/_{B}$ . Note that the cross-terms are suppressed. The implementation of the Choi-Williams distribution used in this work was established by [41].

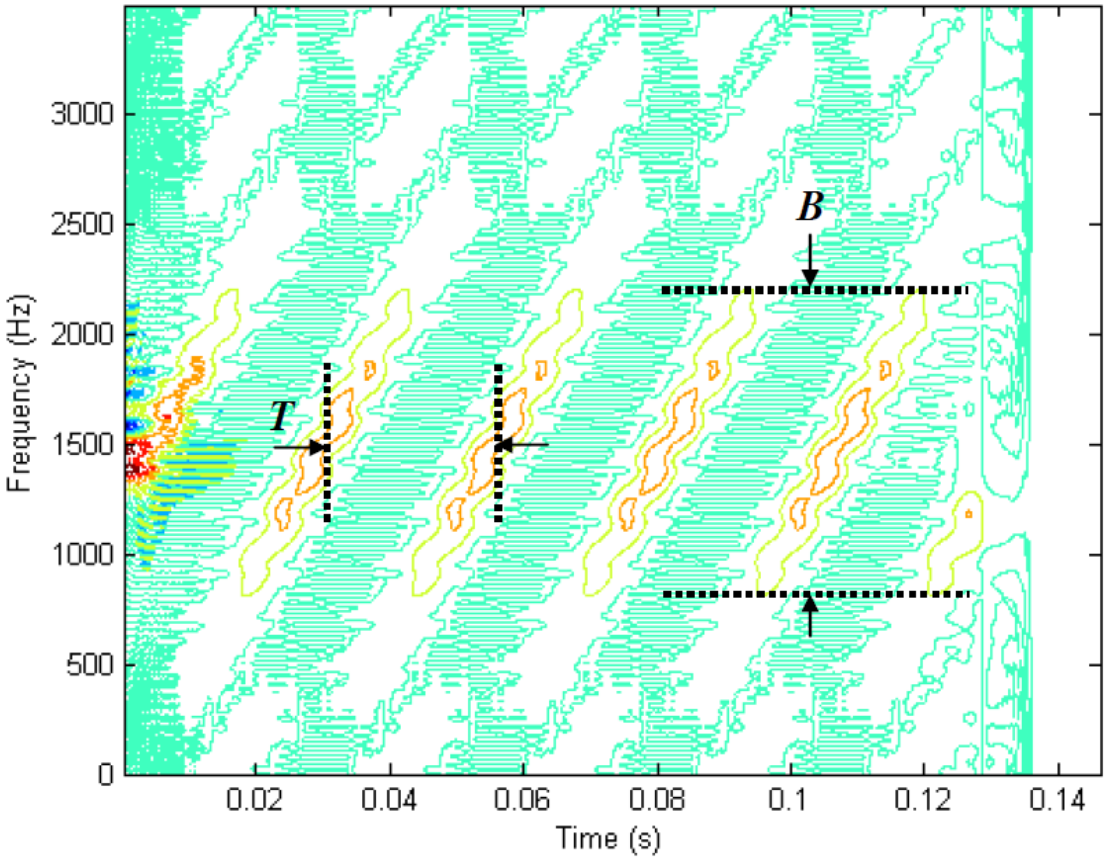


**Figure 3.3: Choi-Williams Distribution of FM-CW Signal [41].**

### 3.3 QUADRATURE MIRROR FILTER BANK TREE

A QMFB tree consists of a number of layers of fully connected pairs of orthogonal wavelet filters (or basis functions) that linearly decompose the received waveform into tiles on the time-frequency plane. A modified sync filter is used and every filter output is connected to a filter pair in the next layer, as shown in Figure 3.4 [40]. Figure 3.4 also illustrates the implementation of the QMFB tree.

The tiles are used to refer to the rectangular regions of the time-frequency plane containing the basis function's energy. Each filter pair divides the digital input waveform into its high-frequency and low-frequency components, with a transition centered at $\pi$. Within the series of time-frequency layers, each subsequent layer provides a trade-off in time and frequency resolution. By examining the energy within the tiles, parameters such as bandwidth, center frequency, phase modulation, signal duration and location in the time-frequency plane can be determined [1].

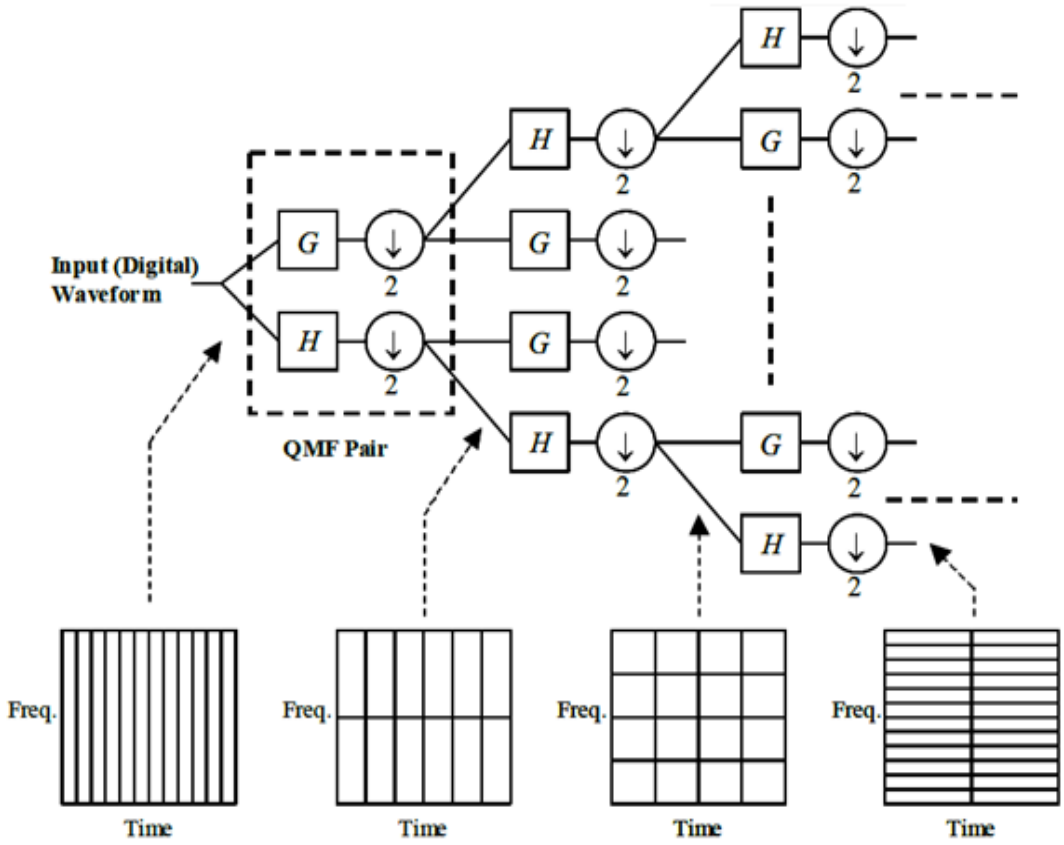


**Figure 3.4: Quadrature Mirror Filter Bank Tree [40].**

The received signal is first padded with zeros to contain $N_p = 2^L$ samples where $L$ is the number of layers within the tree. A normalized input of one sample per second is assumed, with a signal bandwidth of $(0, \pi)$ radians, with $\pi$ corresponding to half the sampling frequency. Since each filter's output signal has half the bandwidth, only half the samples are required to meet the Nyquist criteria; therefore, these sequences are downsampled by two and the same number of output samples is returned [40]. The $L \leq \left[{}^{L}/_{2}\right]$ layer provides a good compromise in time and frequency resolution. The frequency resolution of a QMFB layer $l$ is [1]:

$$\Delta f = \frac{F_s}{2(2^l - 1)} \tag{3.9}$$

where $F_s$ is the sampling frequency. The resolution in time is determined by how many samples are used within the QMFB and is given by:

$$\Delta t = \frac{2^L}{F_s(2^{L-l} - 1)} \tag{3.10}$$

where $L$ is the total number of layers [1].

Figure 3.5 shows the QMFB result for layer $l = 5$ for a FM-CW signal with a carrier frequency of $F_c = 1495$ with a sampling frequency of $F_s = 8\,KHz$. With the number of carrier frequency cycles within a sub code of $cpp = 1$, the transmitted bandwidth $B = \frac{F_c}{cpp} = 1495\,Hz$ and the code period is $T = 8.6\,ms$. Here $L = 10$, $\Delta t = 0.0047\,s$ and $\Delta f = 112.9\,Hz$.

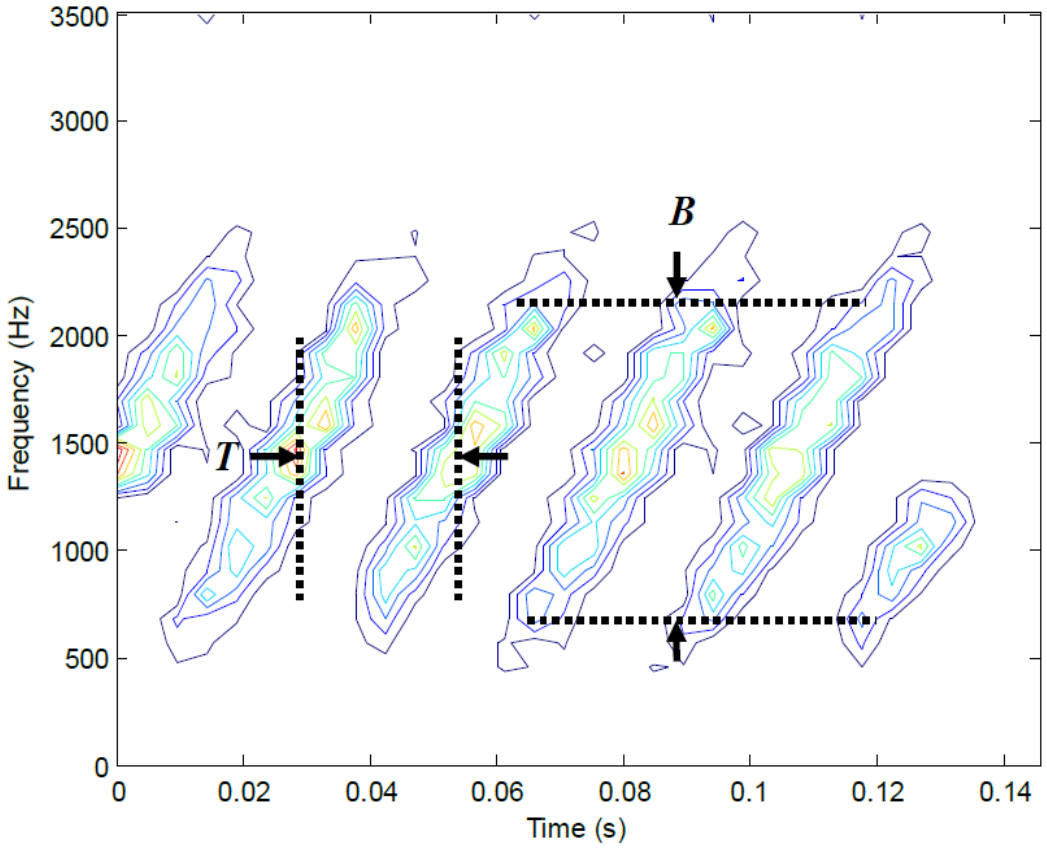


**Figure 3.5: QMFB Result for Layer $l = 5$ for a FM-CW signal [40].**

### 3.4 AUTONOMOUS PREPROCESSING

Autonomous preprocessing is performed in order to generate a feature vector from the T-F images to be used in the classification networks. The first goal of the algorithm is to autonomously crop a part of the image where the signal is present. This is the part of the image within the frequency band of interest [18]. The frequency bands of interests are illustrated in Figure 3.6 between the dash lines.

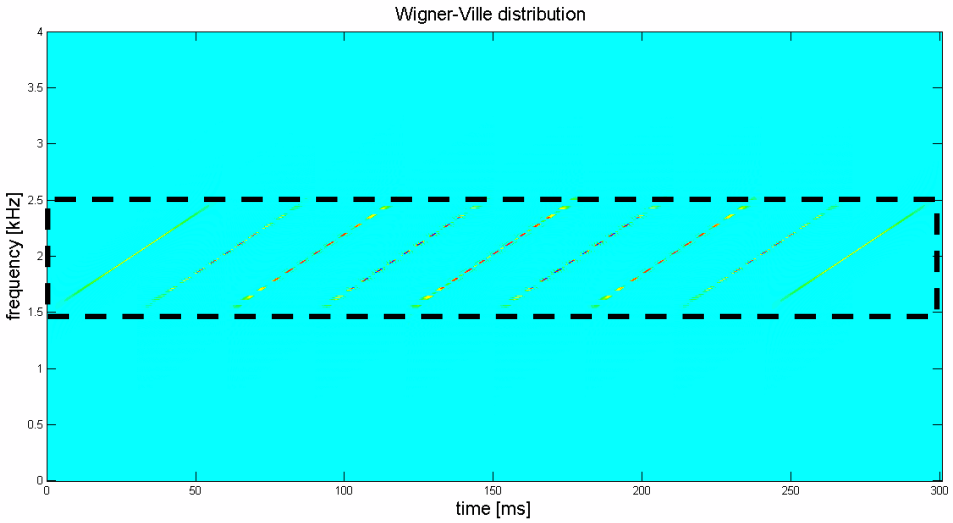


**Figure 3.6: The Frequency Bands of Interests of PWVD.**

The sensitivity of the cropping is very important since the noise level present in the signal may easily distort the algorithm. The less the cropping algorithm is affected by the SNR changes, the more accurate the expected classification results.

The second goal is to process the images with minimum interference (for instance thresholding, binarization, morphological operations, etc.). Any operation on the images either adds new information to the image or results in some information loss [44]. The third goal is to reduce the dimension of the feature vectors while preserving their discriminating properties.

T-F representations are processed as images throughout this work. Let the dimension of an image be $M \times N$. In this work for the PWVD image $M, N$ depends on the length of the intercepted signal sequence, which is the sample size. Following sections briefly explain each step taken through T-F autonomous cropping and feature extraction operations.

## 3.5 T-F AUTONOMOUS CROPPING AND FEATURE EXTRACTION ALGORITHM

The block diagram of the T-F autonomous cropping and feature extraction algorithm used in this work is shown in Figure 3.7.

The first step of the algorithm is to detect and delete the region where no signal is present. No signal regions may occur if the duration of the FM-CW signal is smaller than

the time interval processed. The block corresponds to this step is shown in Figure 3.8. This step is performed as defined in [45].

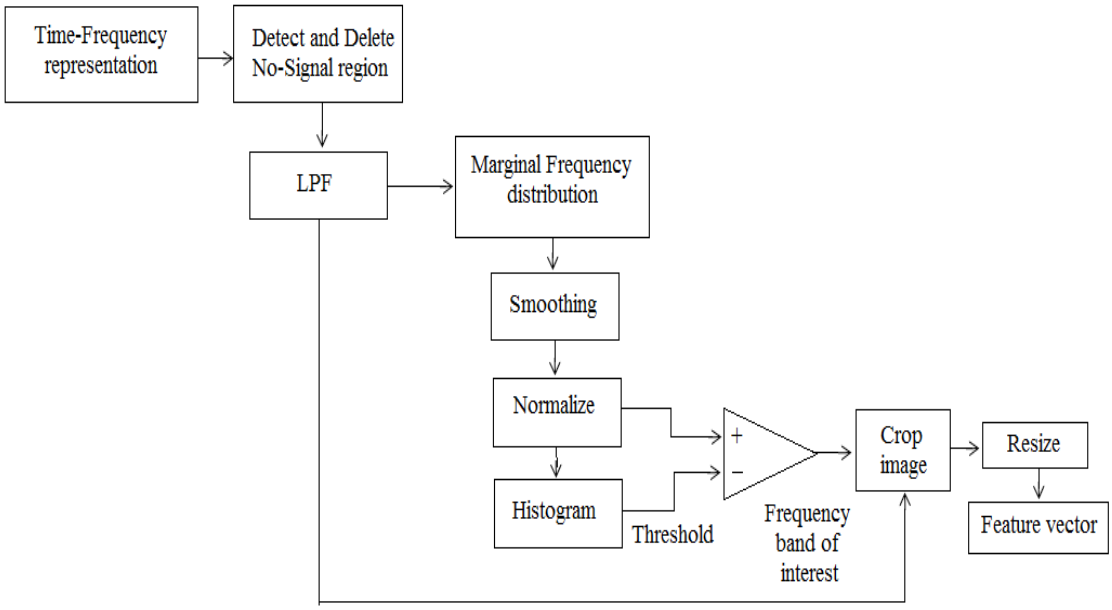


**Figure 3.7: T-F Autonomous Cropping and Feature Extraction Algorithm [18].**

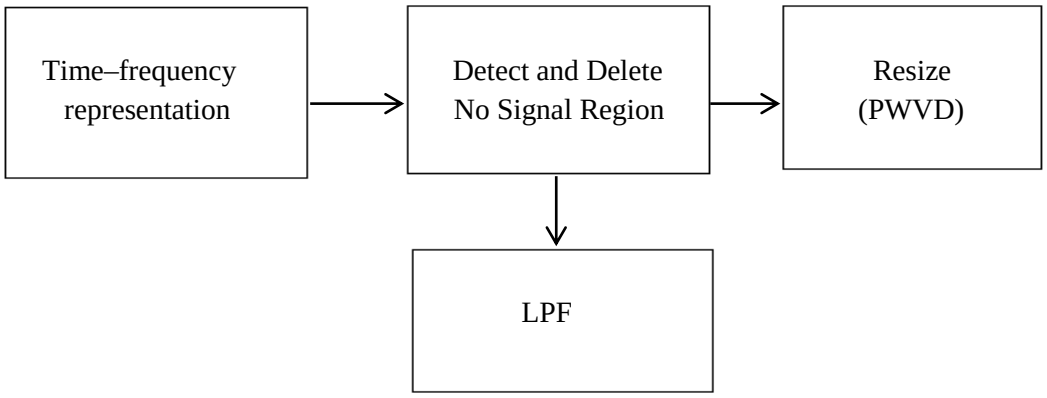


**Figure 3.8: Detect and Delete "No-signal region" Block [45].**

Figure 3.9 shows an illustration of this operation. The image is obtained by WVD representation of FM-CW signal with $F_s = 8\,KHz$, $F_c = 2000\,Hz$ and $cpp = 1 (B = 2000\,Hz)$ with an $SNR = 0\,dB$. Figure 3.9 $(a)$ shows the original output of the WVD, and Figure 3.9 $(b)$ shows the new image after the no-signal region is deleted.

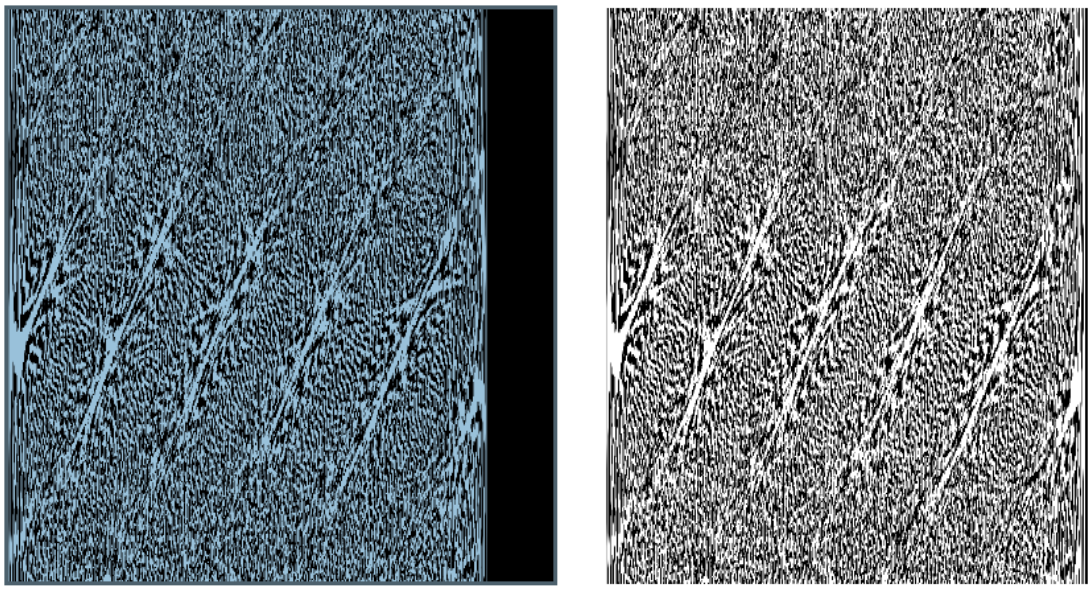

$(a)$ $(b)$

**Figure 3.9: (a) T-F Image with No-Signal Region (b) Image after No-Signal Region Cropped.**

Followed by the deletion of the no-signal region, the image is lowpass filtered (LPF). Assuming that the additive noise has high frequency components and the LPI modulation energy is preserved in the low frequencies, after filtering only the modulation energy should be preserved. The filtering can be performed in the frequency domain [18].

## 3.6 The 2-D Discrete Fourier Transform and Frequency Domain Filtering

Let $f(k_1, k_2)$, for $k_1 = 0,1,2 \ldots\ldots, M-1$ and $k_2 = 1,2,3 \ldots, N-1$, denote an $M \times N$ image. The 2-D DFT of $f$, denoted by $F(u, v)$, , is given by [42] :

$$F(u,v) = \sum_{k_1}^{M-1} \sum_{k_2}^{N-1} f(k_1, k_2) e^{-j2\pi\left({}^{uk_1}/_{M} + {}^{vk_2}/_{N}\right)} \qquad (3.11)$$

for $u = 1,2,3 \ldots\ldots, M-1$ and $v = 1,2,3 \ldots\ldots, N-1$. The frequency domain is simply the coordinate system spanned by $F(u, v)$ with $u$ and $v$ as variables. The $M \times N$ rectangular region defined by $u$ and $v$ is often referred as the frequency rectangle and of the same size as the input image. Note that frequency rectangle can an also be defined by digital frequencies as shown in Figure 3.10.

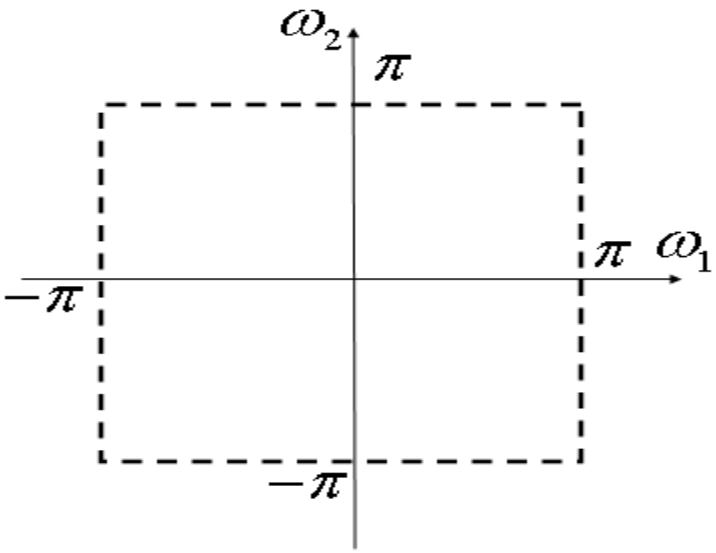


**Figure 3.10: Frequency Rectangle Defined by Digital Frequencies [46].**

where $\omega_1 = u2\pi/M$ and $\omega_2 = v2\pi/N$.

Given $F(u,v)$, $f(k_1,k_2)$ can be obtained by means of the inverse DFT. Both DFT and inverse DFT are obtained in practice using a Fast Fourier transform (FFT) algorithm [42].

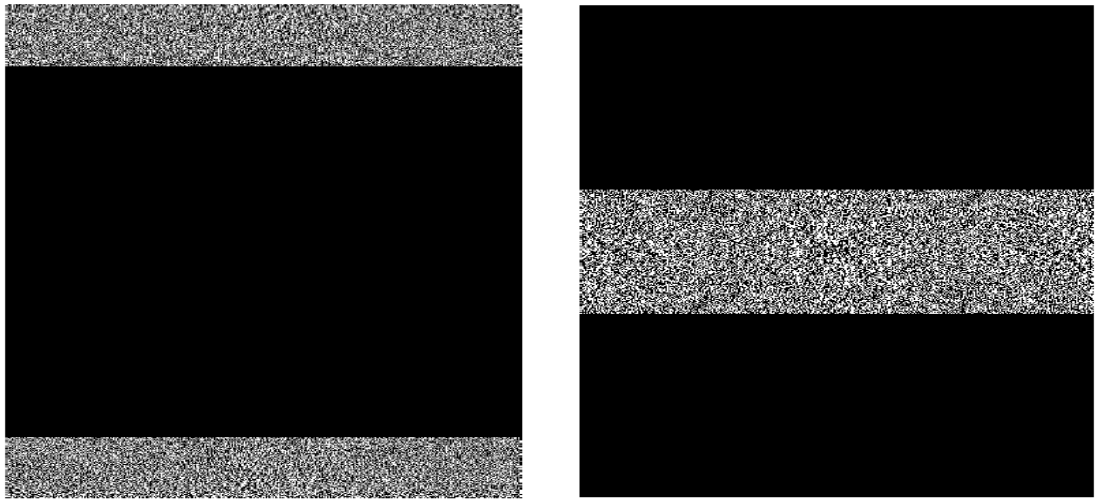

**(a)** **(b)**

**Figure 3.11: (a) 2-D FFT of image shown in Figure 3.9 (b)**
**(b) The zero frequency component is shifted to the center of spectrum.**

If $f(k_1, k_2)$ is the image obtained by WVD representation of a FM-CW signal with a carrier frequency of $F_c = 1495\,Hz$ with a sampling frequency of $F_s = 8KHz$ and $cpp = 1$ with an $SNR = 0dB$, the 2-D FFT of $f(k_1, k_2)$ is shown in Figure 3.11 (a) and the zero frequency component shifted to the center of spectrum is shown in Figure 3.11 (b).

The convolution theorem which is the foundation for linear filtering in both spatial and frequency domains can be written as follows [42]:

$$f(k_1, k_2) * h(k_1, k_2) \Leftrightarrow H(u, v) * F(u, v) \tag{3.12}$$

The filtering in the spatial domain consists of convolving an image $f(k_1, k_2)$ with a filter mask, $h(k_1, k_2)$ According to the convolution theorem; the same result can be obtained in the frequency domain by multiplying $H(u, v)$ by $F(u, v)$ which can also be referred as the *filter transfer function* [42]. The frequency domain filtering used in this work is shown in Figure 3.12.

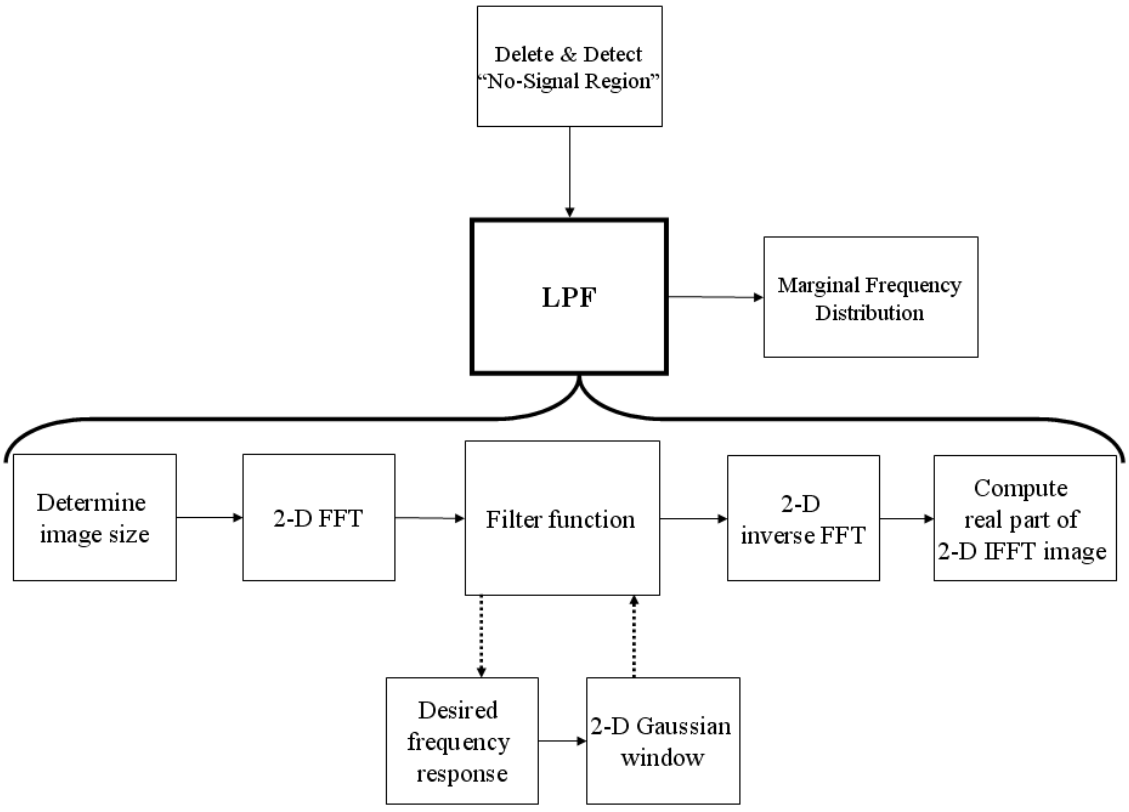


**Figure 3.12: Frequency Domain Filtering Operations [42].**

In this work $H(u,v)$ is obtained in three steps. First, the desired frequency response (ideal lowpass filter) $H_d(u,v)$ is created as a matrix. An ideal lowpass filter has the transfer function [42]:

$$H_d(u,v) = \begin{cases} 1 \; if \; D(u,v) \leq D_0 \\ 0 \; if \; D(u,v) \geq D_0 \end{cases} \tag{3.13}$$

where $D_0$ (cutoff parameter) is a specified nonnegative number and $D(u,v)$ is the distance from point $(u,v)$ to the center of the filter. $D_0$ can also be defined as the normalized value of digital frequencies $\omega_1, \omega_2$ by $\pi$.

Second, a two dimensional Gaussian window is created with a standard deviation [42]:

$$\sigma = N \times D_0/8 \tag{3.14}$$

where $N$ is the number of columns in the image. Since the standard deviation of the window is related to $D_0$, the structure becomes adaptive to the changes in the desired frequency response. In this application, both the frequency response matrix and the Gaussian window have dimensions of $M \times N$ which is equal to the image dimension $f(k_1, k_2)$ and the 2-D FFT output dimension $F(u,v)$. The last step is to multiply $H_d(u,v)$ by the Gaussian window.

The transfer function of the Gaussian lowpass filter obtained by this multiplication process is then given by [42]:

$$H(u,v) = e^{D^2(u,v)/2\sigma^2} \tag{3.15}$$

These steps are illustrated in Figure 3.13 Figure 3.13 (a) shows the desired frequency response with $D_0 = 0.3$ (where $|D_0| \in 0,1$) or $\omega_1 = \omega_2 = 0.3\pi$, Figure 3.13 (b) shows the Gaussian window with $\sigma = N \times D_0/8 = 33.825$. The dimension of both the frequency response matrix and Gaussian window is $M = 1024$ and $N = 902$. Figure 3.13 (c) shows the resultant Gaussian lowpass Filter and Figure 3.13 (d) shows the Gaussian lowpass filter as an image. Several values of $\omega_1, \omega_2$ are tested during the simulation to find an optimum value for each distribution. For each trial, the digital cutoff frequencies are set to be $\omega_1 = \omega_2$.

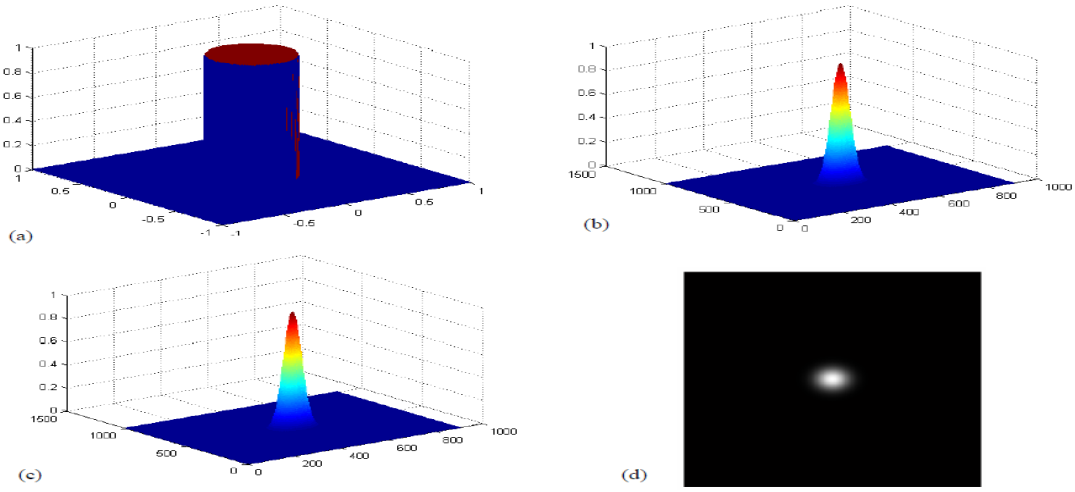


**Figure 3.13: Implementation of Filter Function (a) Desired Frequency Response, (b) Gaussian Window, (c) Gaussian Lowpass Filter, (d) Gaussian Lowpass Filter as an image.**

After obtaining the lowpass filter, the frequency domain filtering can be implemented by multiplying $F(u,v)$ by $H(u,v)$. This operation is followed by shifting back of the frequency components and taking the inverse FFT of the filtered domain. The last step is obtaining the real part of the inverse FFT. Figure 3.14 illustrates these steps. Figure 3.14 (a) shows the result after the frequency domain filtering of Figure 3.9 (b), Figure 3.14(b) shows decentering of the frequency components and Figure 3.14 (c) shows the real part of the 2-D inverse FFT.

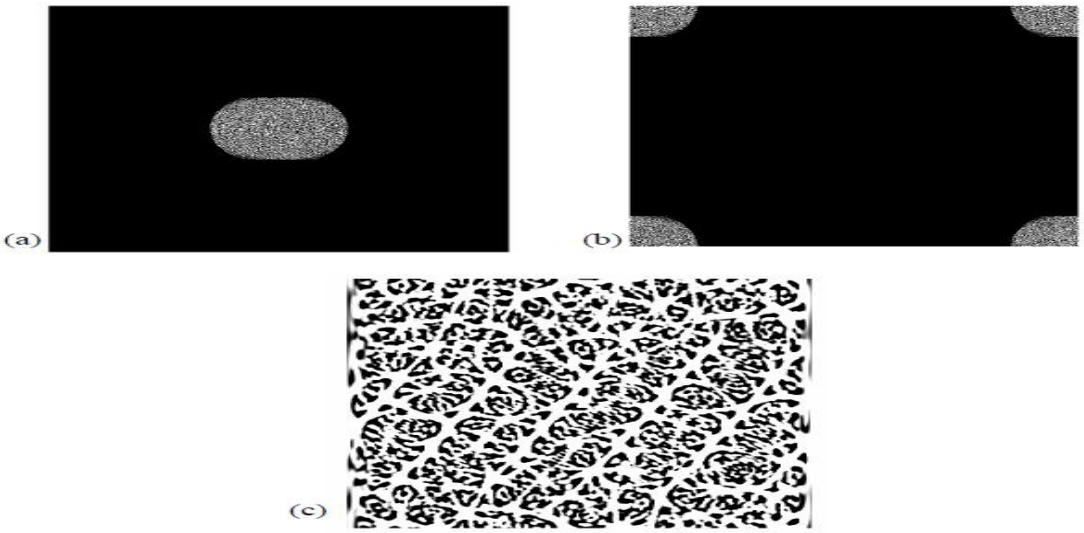


**Figure 3.14: (a) Frequency Domain Filtering, (b) Shift Back the Frequency Components, (c) 2-D Inverse FFT output.**

### 3.7 DETERMINATION OF THE FREQUENCY BAND OF INTEREST

The steps for determining the frequency band of interest from the T-F plane is shown in Figure 3.15. The operations are applied to the marginal frequency distribution (MFD) of the T-F plane. The MFD gives the instantaneous energy of the signal as a function of frequency. This is obtained by integrating the time values for each frequency in the T-F image resulting $M \times 1$ values.

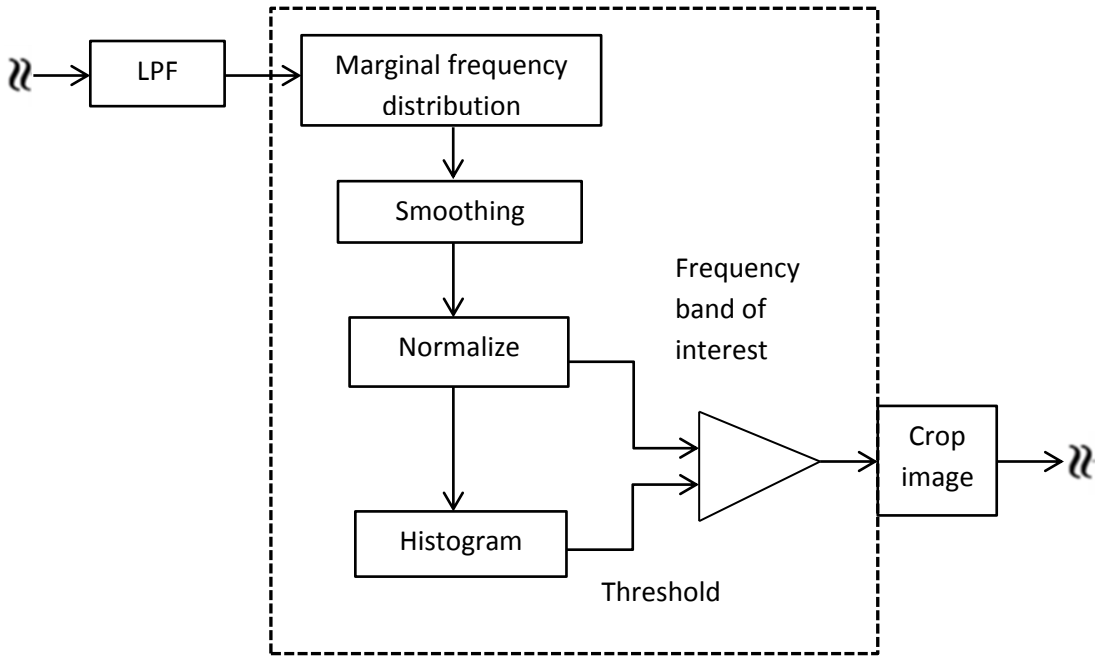


**Figure 3.15: Determining the Frequency Band of Interest [18].**

The MFD of a FM-CW coded signal with $F_s = 8$ KHz, $F_c = 2000$ Hz, and $cpp = 1$ ($B = 2000$ Hz) with an $SNR = 0dB$ is shown in Figure 3.16.

As it can be seen from the Figure 3.16 the higher energy interval corresponds to the frequency band of interest which preserves the modulation energy. The goal is to isolate and crop the region of interest as accurately as possible. This is done by setting a threshold. The instantaneous energy values above the threshold can be collected and cropped. But one problem will emerge as the noise level changes; the actual position set by the threshold may change from one SNR level to another. In order to minimize this effect, a smoothing operation is applied [18].

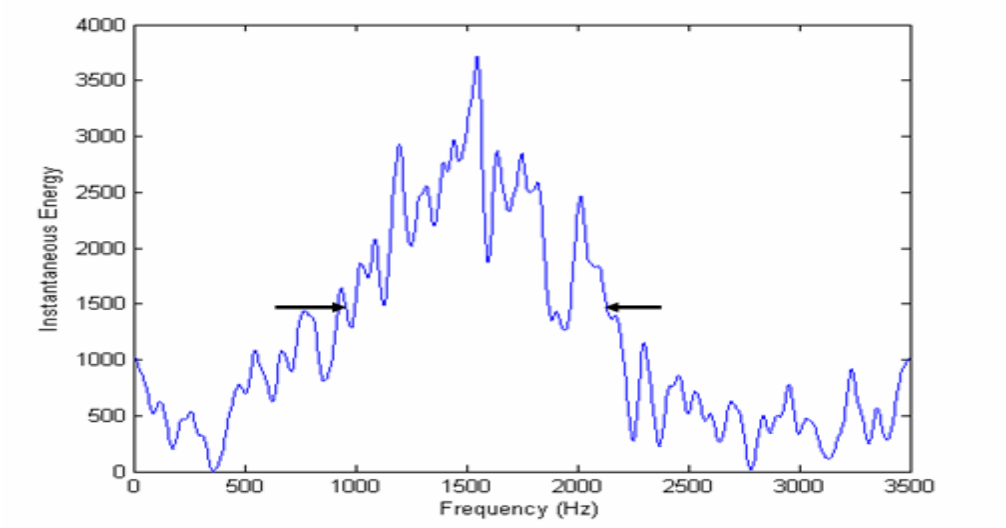


**Figure 3.16: Marginal Frequency Distribution (MFD) of a FM-CW Signal [18].**

The smoothing is applied in two steps as shown in Figure 3.17. In the first step an adaptive filter is applied to attenuate the noise. In the second step a moving average filter is applied to smooth the edges and local peaks.

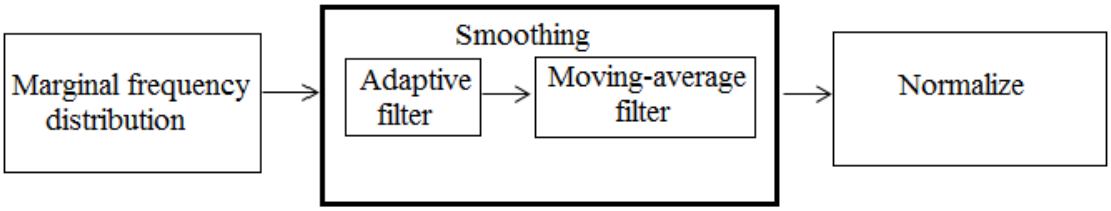


**Figure 3.17: MFD Smoothing via Adaptive Filter & Moving-Average Filter [18].**

An adaptive filter is a filter that changes behavior based on the statistical characteristics of the input signal within the filter. In this work a Wiener filter is applied using the local neighborhood of size m-by-1 to estimate the local image mean and standard deviation. The filter estimates the local mean and variance around each vector element. The local mean is estimated as [18]:

$$\mu = \frac{1}{m}\sum_{n\in\eta} \mathrm{A}(n) \tag{3.16}$$

and the local variance is estimated as follows:

$$\sigma^2 = \frac{1}{m}\sum_{n=\eta} \mathrm{A}^2\,(n) - \mu^2 \tag{3.17}$$

where $\eta$ is the $m$-by-1 local neighborhood of each element in the vector A. The processed image within the local neighborhood can be expressed as:

$$b(n) = \mu + \frac{\sigma^2 - v^2}{\sigma^2}(\mathrm{A}(n) - \mu) \tag{3.18}$$

where $v^2$ is the noise variance estimated using the average of all the local estimated variances. When the variance is large, the filter performs little smoothing and when the variance is small, it performs more smoothing.

For PWVD images a local neighborhood of $\eta = 10$ is used. Figure 3.18 shows the output of the adaptive filter for the input MFD of FM-CW signal. Note that there is considerable noise attenuation.

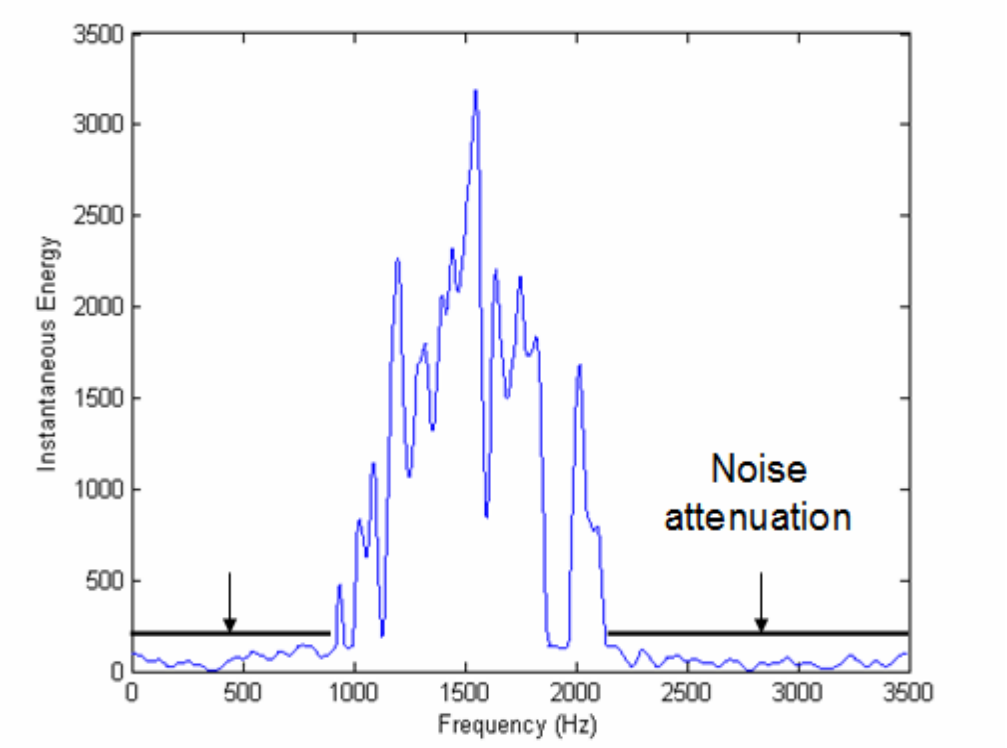


**Figure 3.18: MFD of a FM-CW Signal after Adaptive Filtering [18].**

Although the adaptive noise attenuation gives promising results, the threshold determination may be affected by the local noise peaks that could not be reduced by the adaptive filter. To avoid this problem a moving average filter is applied to the output of the adaptive filter. As a generalization of the average filter, averaging over $N + M + 1$ neighboring points can be considered. The moving average filter is represented by the following difference equation [23].

$$y(n) = \frac{1}{N+M+1}\sum_{k=-N}^{M} x\,(n-k) \tag{3.19}$$

where $x(n)$ is the input and $y(n)$ is the output. For PWVD a window length of $N + M + 1 = 10$ is used. Figure 3.19 shows $\widetilde{\mathrm{A}}_{avg}$, the output vector of the moving average filter with $N + M + 1 = 10$.

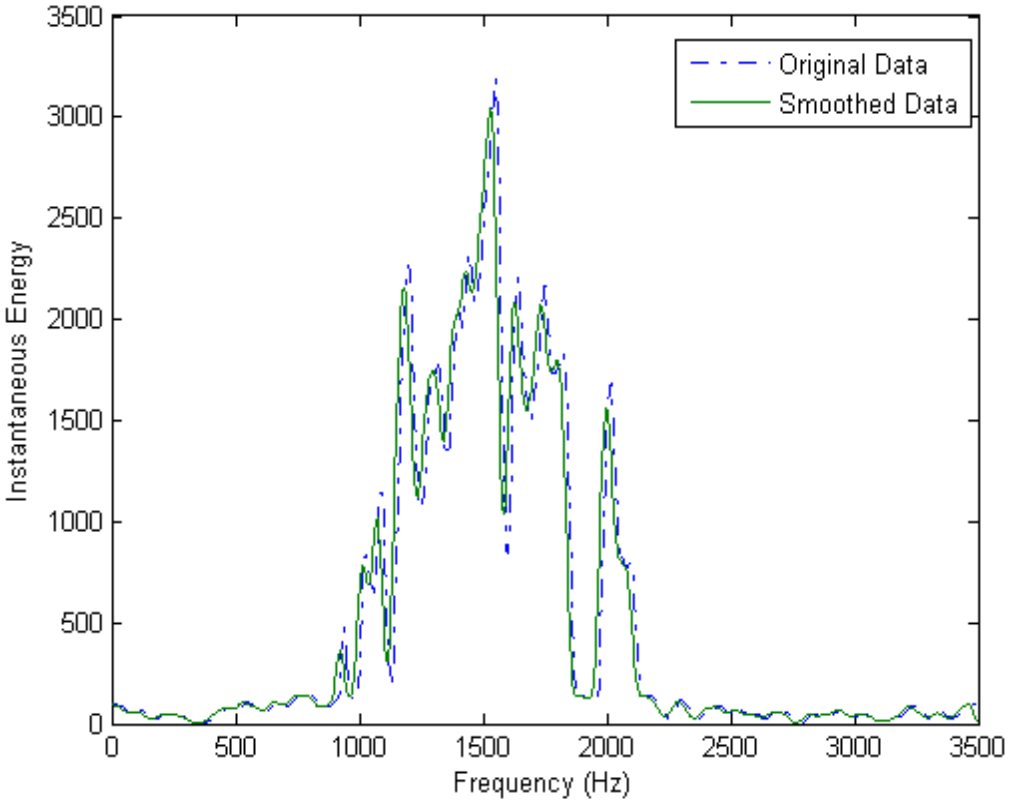


**Figure 3.19: Output of Moving Average Filter with a Window Length of 10 [23].**

After moving average filtering, the output is normalized by the maximum value of $\widetilde{\mathrm{A}}_{avg}$ as follows:

$$\mathrm{A}_n = \frac{\widetilde{\mathrm{A}}_{avg}}{max(\widetilde{\mathrm{A}}_{avg})} \tag{3.20}$$

where $\mathrm{A}_n$ is the normalized smoothed MFD. After normalization a histogram of 100 bins is generated for PWVD images. Using these histogram bins a threshold is determined [6]. Threshold determination is illustrated in Figure 3.20 using the histogram of $\mathrm{A}_n$ for the 30th bin. Note that the value corresponding to the 30th bin, $T_h = 0.2954$ is selected as the threshold.

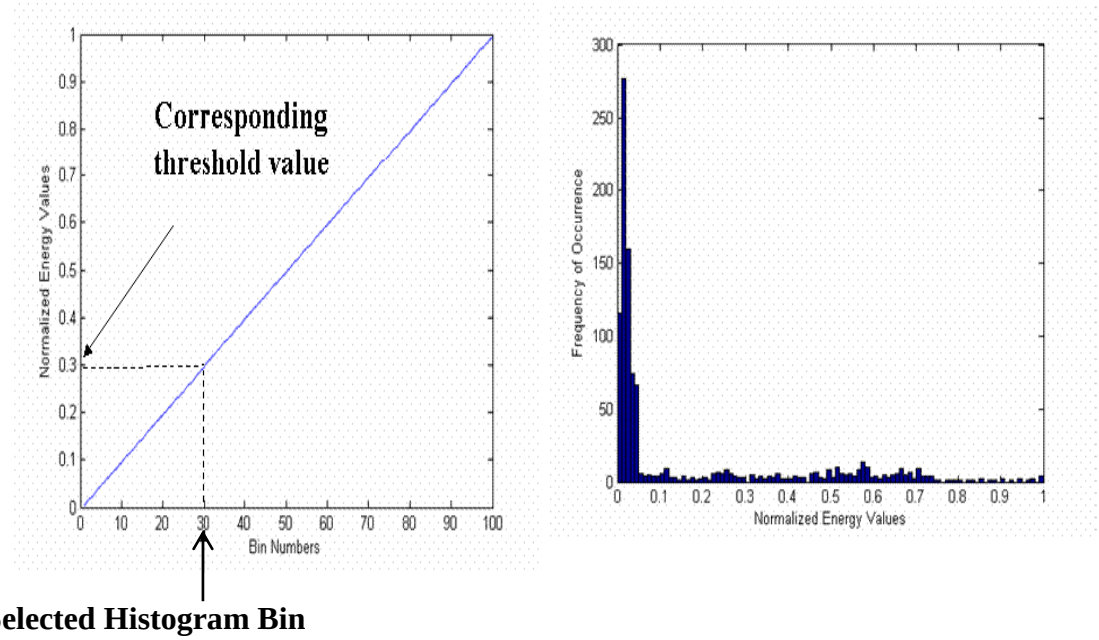


**Figure 3.20: Threshold Determination by a Histogram.**

Once the threshold is determined, the values of $A_n$ below the threshold are set to zero. Then the beginning and ending frequencies of the frequency band of interest is determined as shown in Figure 3.21. Using the lowest and highest frequency values from the frequency band of interest the modulation energy can now be cropped from the image.

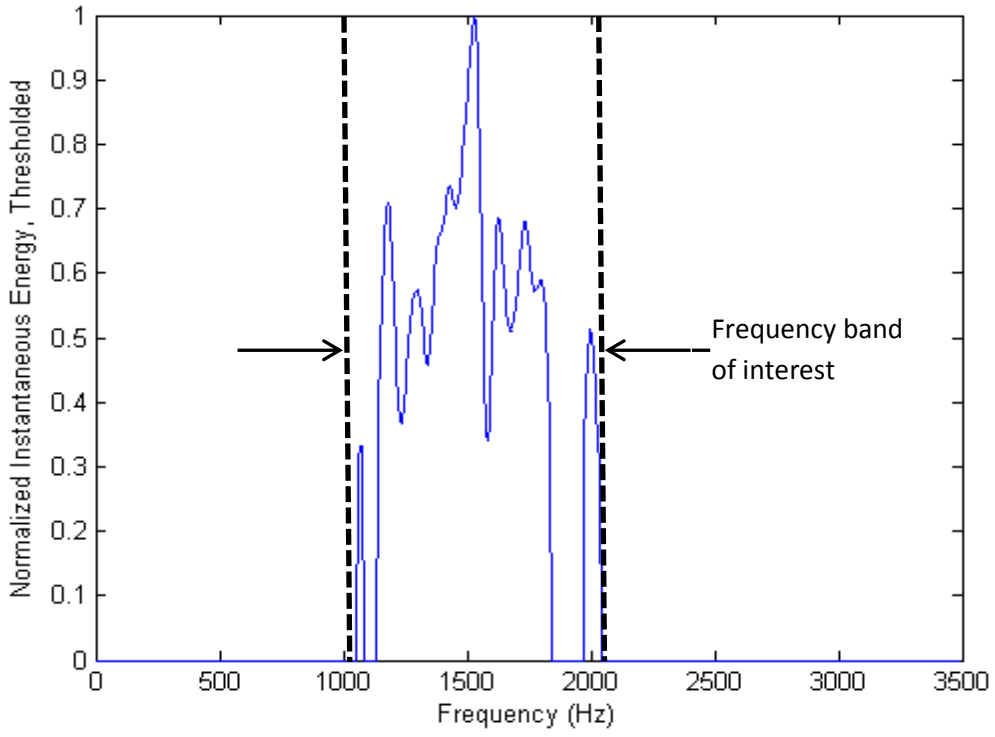


**Figure 3.21: Frequency Band of Interest [6].**

# CHAPTER 4
# PARAMETER EXTRACTION ALGORITHM

Parameter extraction is the last phase of FM-CW signal detection and classification algorithm. Once the signal modulation is identified, the parameters of the signal should be extracted to counter attack the transmitting systems.

In this work, one parameter extraction algorithms is investigated. The algorithm extracts the parameters of FM-CW radar using the PWVD images. The extracted parameters are the carrier frequency $F_c$, bandwidth $B$ and code period $T$.

The illustrations presented in this section are based on FM-CW signal with carrier frequency of $F_c = 2000\ Hz$, sampling frequency of $F_s = 8\ KHz$ at an SNR level of 0 $dB$. With the number of carrier frequency cycles within a subcode of $cpp = 1$, the transmitted bandwidth $B = {F_c}/{cpp} = 2000\ Hz$ and the code period is $T = 8.6\ ms$.

## 4.1 PARAMETER EXTRACTION OF FM-CW RADAR USING PWVD IMAGES

The parameter extraction algorithm for FM-CW radar waveforms using PWVD images is shown in Figure 4.1.

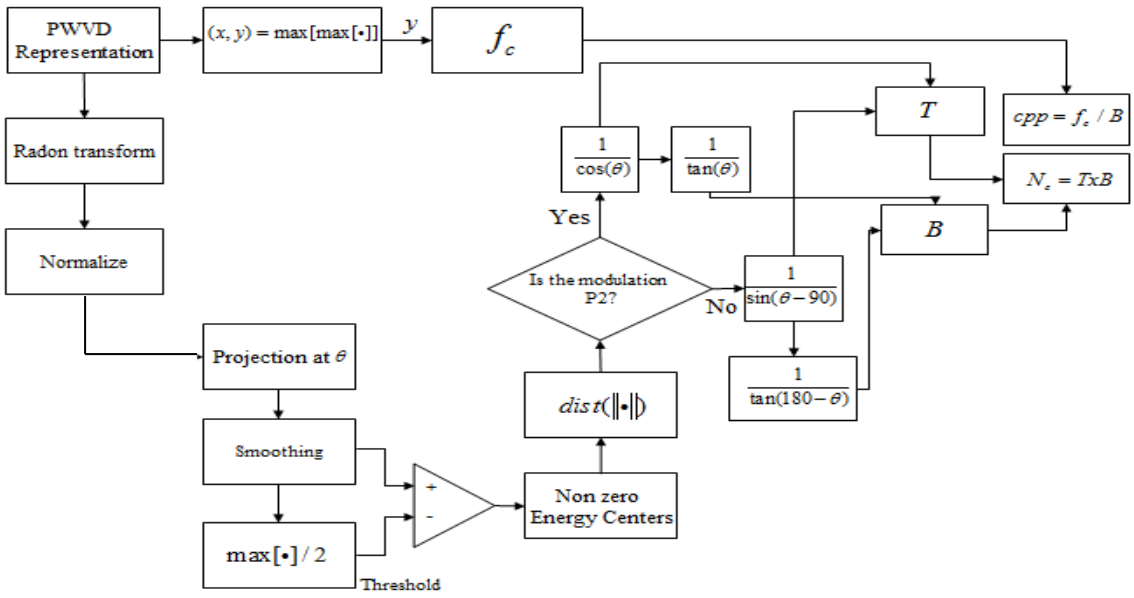


**Figure 4.1: Parameter Extraction Block Diagram of FM-CW Radar Waveforms using PWVD images [18].**

The algorithm carrier frequency $F_c$ is extracted directly from the PWVD image without any pre-processing. This is performed by finding the location of the maximum intensity level in the image. The corresponding frequency at this location gives $F_c$ [18]. This is illustrated in Figure 4.2 on a grayscale PWVD image. Note that with the PWVD, this maximum sometimes occurs at a cross term but not all the times.

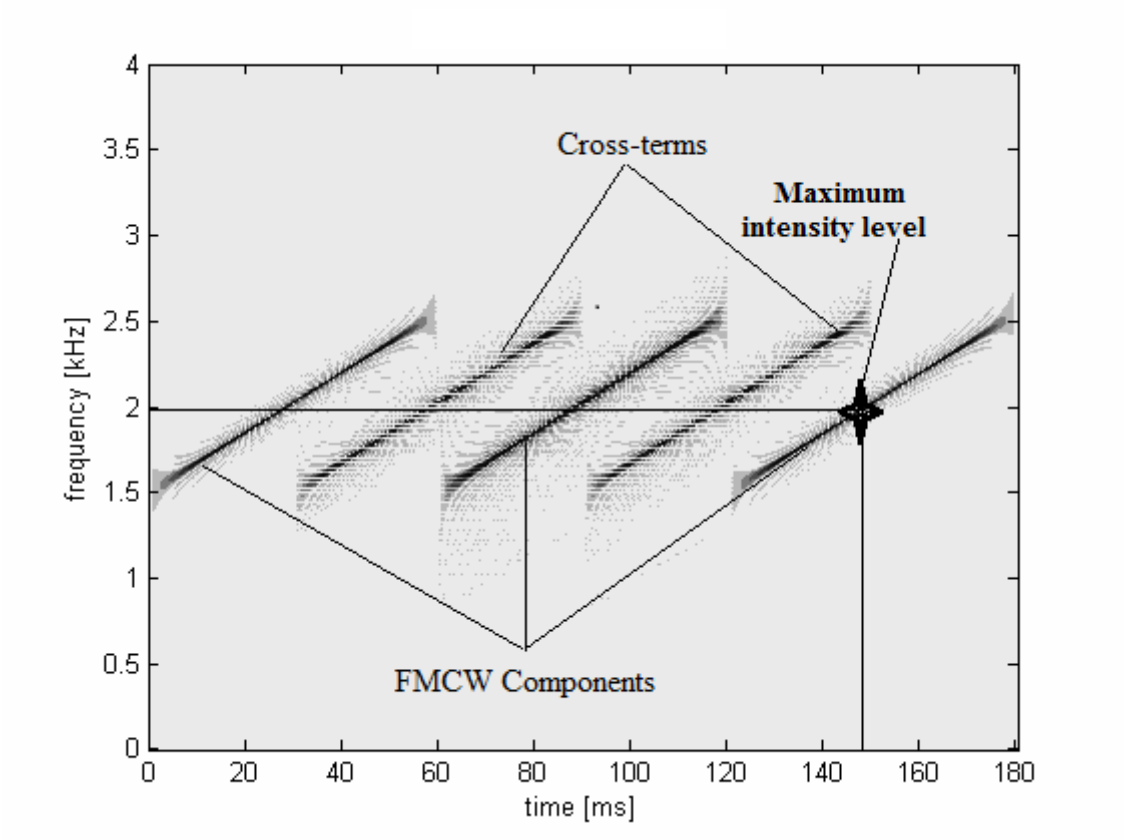


**Figure 4.2: Carrier Frequency Determination by Finding the Maximum Intensity Level from PWVD.**

## 4.2 RADON TRANSFORM

In order to extract the code length $T$ and bandwidth $B$, the Radon transform of the image is computed [18]. The Radon transform is the projection of the image intensity along a radial line oriented at a specific angle, it transforms a 2-D image with lines (line-trends) into a domain of the possible line parameters $\rho$ and $\theta$, where $\rho$ is the smallest distance from the origin and $\theta$ is its angle with the x-axis. In this form, a line is defined as [46].

$$\rho = x\cos\theta + y\sin\theta \tag{4.1}$$

Using this definition of a line, the Radon transform of a 2-D image $f(x, y)$ can then be defined as follows:

$$\mathrm{R}(\rho, \theta) = \int_{-\infty}^{\infty} f(\rho cos\theta - ssin\theta, \rho sin\theta + cos\theta) ds \tag{4.2}$$

where the *s*-axis lies along the line perpendicular to $\rho$ as shown in Figure 4.3. Here, *s* can be calculated from

$$s = ycos\theta - xsin\theta \tag{4.3}$$

Note $\rho$ and $s$ can be calculated from $x$, $y$ and $\theta$ using (4.1) and (4.3).

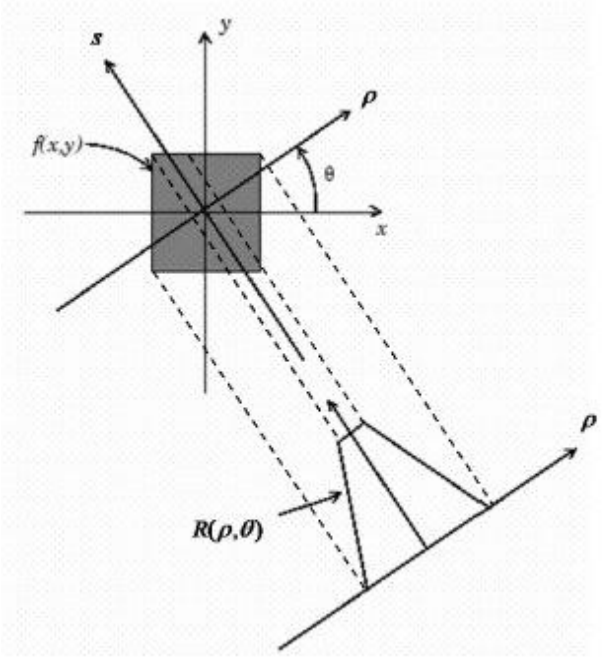


**Figure 4.3: Geometry of the Radon Transform [46].**

In this work, the projection of the images are computed as line integrals from multiple sources along parallel paths in a certain direction. The beams are spaced 1 pixel unit apart. This is illustrated in Figure 4.4 for a single projection at a specified rotation angle $\theta$ [46].

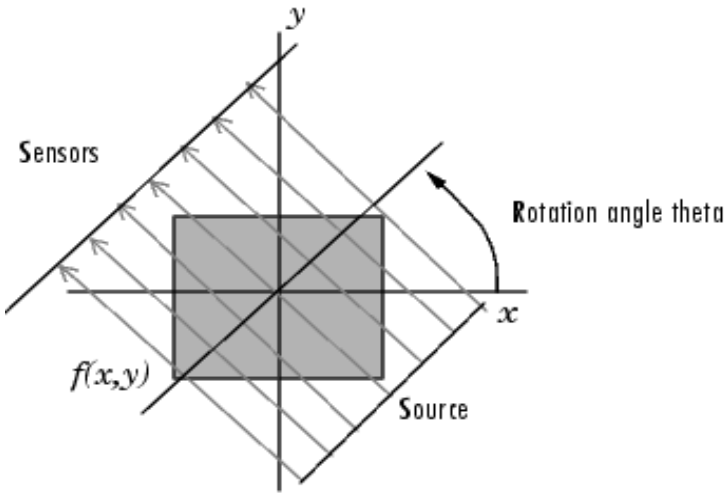


**Figure 4.4: Parallel Beam Projection at Rotation Angle [46].**

Figure 4.5 shows the grayscale PWVD image illustrating the extraction goal for the bandwidth and the code period. The algorithm aims to measure the indicated regions by implementing the Radon transform to find $\theta$ and $d$. Here $d$ is the distance between consecutive linear energy lines of the modulation at angle $\theta$. To prevent confusion the angle $\theta$ which is equal to the slope of the modulation energy lines will be referred as $\theta_0$ for the rest of the section. The expectation is to obtain maximum intensity levels in the transformed image at angle $\theta_0$. Once $\theta_0$ and $d$ is determined, $B$ and $T$ can be calculated using geometrical relations as shown below [18].

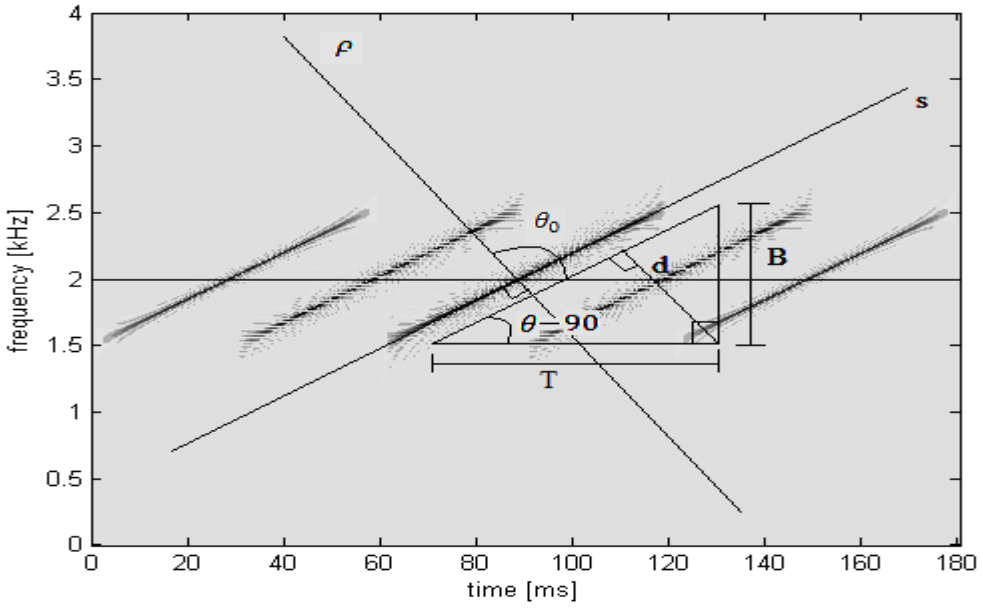


**Figure 4.5: Radon Transform Geometry on PWVD image [18].**

The Radon transform is implemented so that the parallel-beam projections of the image are taken between [0, 179]. Once the transform is completed it is normalized as in [18]. The normalized radon transform of the PWVD image is shown in Figure 4.6 on a contour plot.

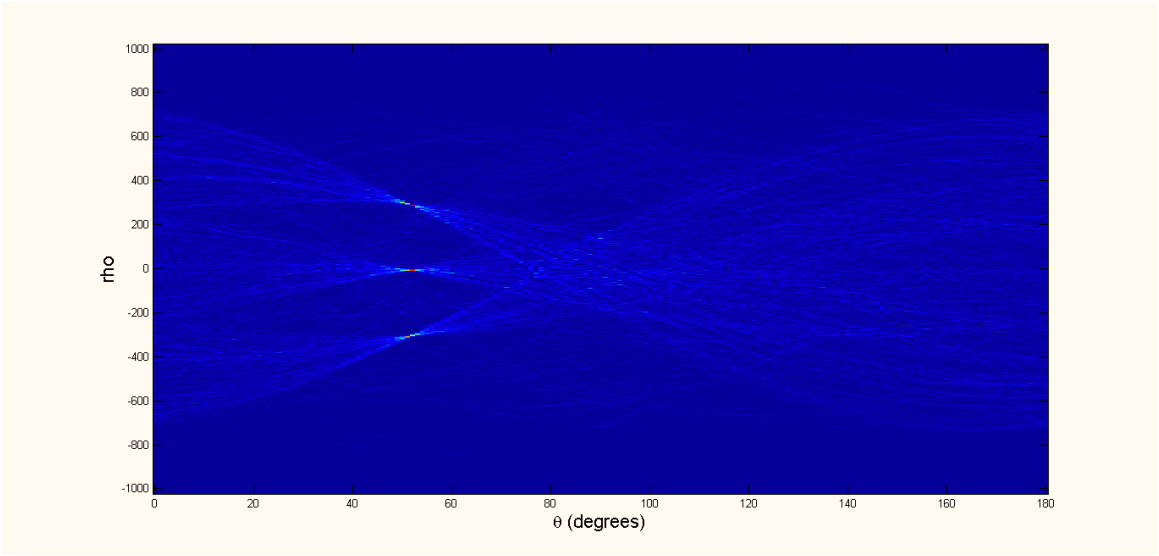


**Figure 4.6: Normalized Radon Transform of a PWVD Image.**

The 3-D mesh plot of Radon transform is shown in Figure 4.7. This shows the number of target present in the signal and the intensity level of the received signal.

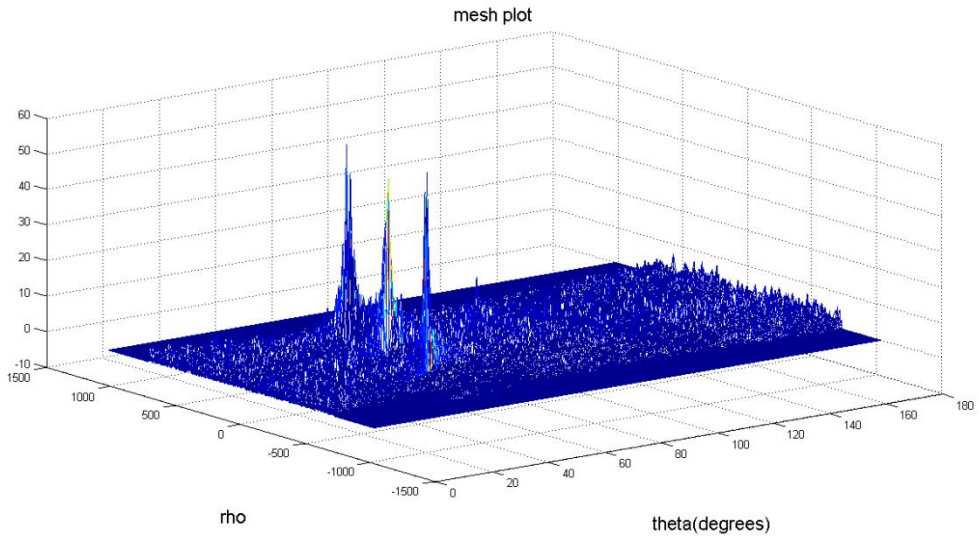


**Figure 4.7: 3-D Mesh plot of Radon Transform of PWVD Image.**

In some cases, the maximum intensity on the transform may occur around $\theta = 90^0$ which corresponds to the marginal frequency distribution (MFD). Since we do not want to detect

the angle corresponding to the MFD, we assume that the slope of linear energy lines are not between $10^0$ and $-10^0$ and the projections on angles between $\theta = [80^0, 100^0]$ are masked, and set to zero. After masking, the location of the maximum intensity level of the transform is found. The corresponding projection angle at this location gives $\theta_0$ [18].

Once $\theta_0$ is found the projection at angle $\theta_0$ is cropped from the masked Radon transform and a projection vector is obtained. Figure 4.8 and figure 4.9 illustrates the cropping of the projection at angle $\theta_0$ from the masked Radon transform.

From Figure 4.8 and Figure 4.9 the number of modulation energy lines contained in the WVD image can easily be detected from both the Radon transform and the projection vector at angle $\theta_0$. The ripples between each modulation energy component correspond to the noise and cross term integration at angle $\theta_0$. As noise increases, these ripples also increase. High levels of noise may affect the thresholding process. Due to this fact the projection vector is smoothed with an adaptive filter using the same algorithm as in the T-F autonomous cropping and feature extraction algorithm [7].

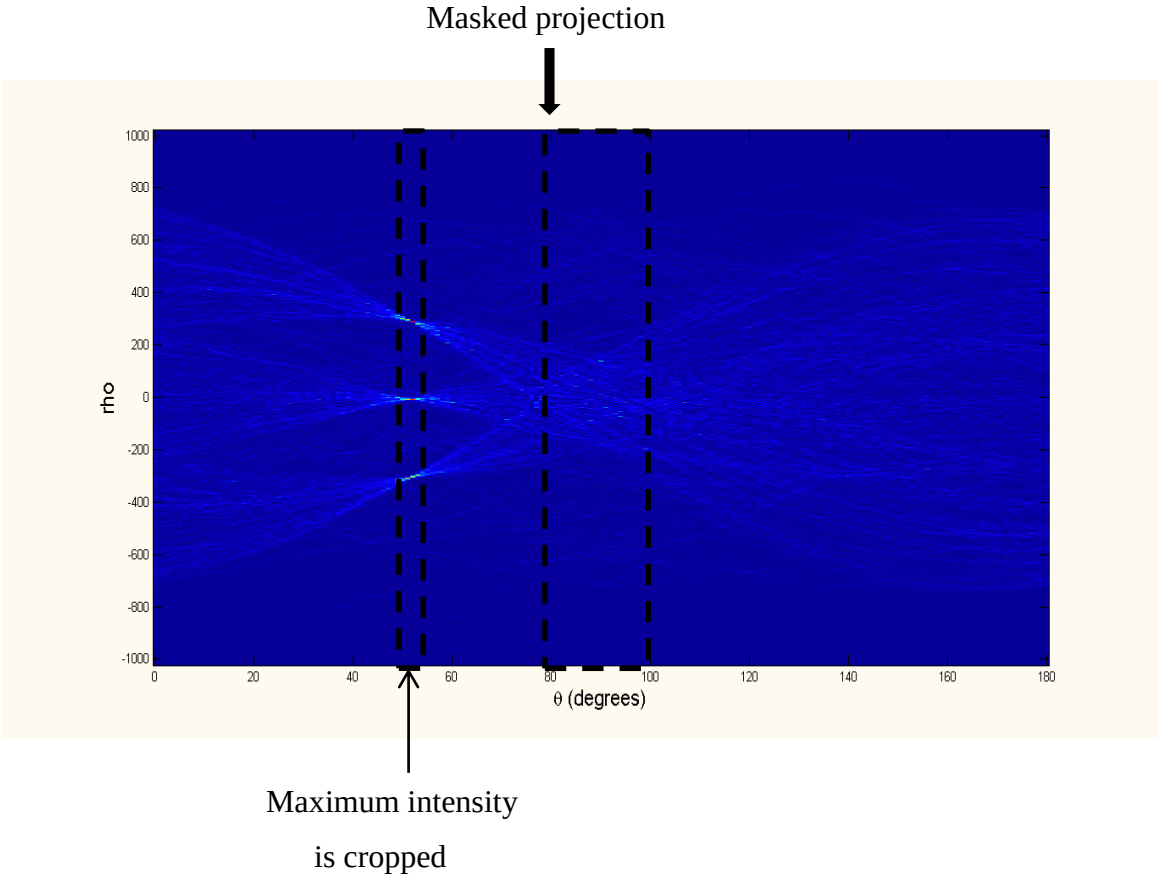


**Figure 4.8: Radon Transform and Vector Cropping on an Angle $\theta_0$.**

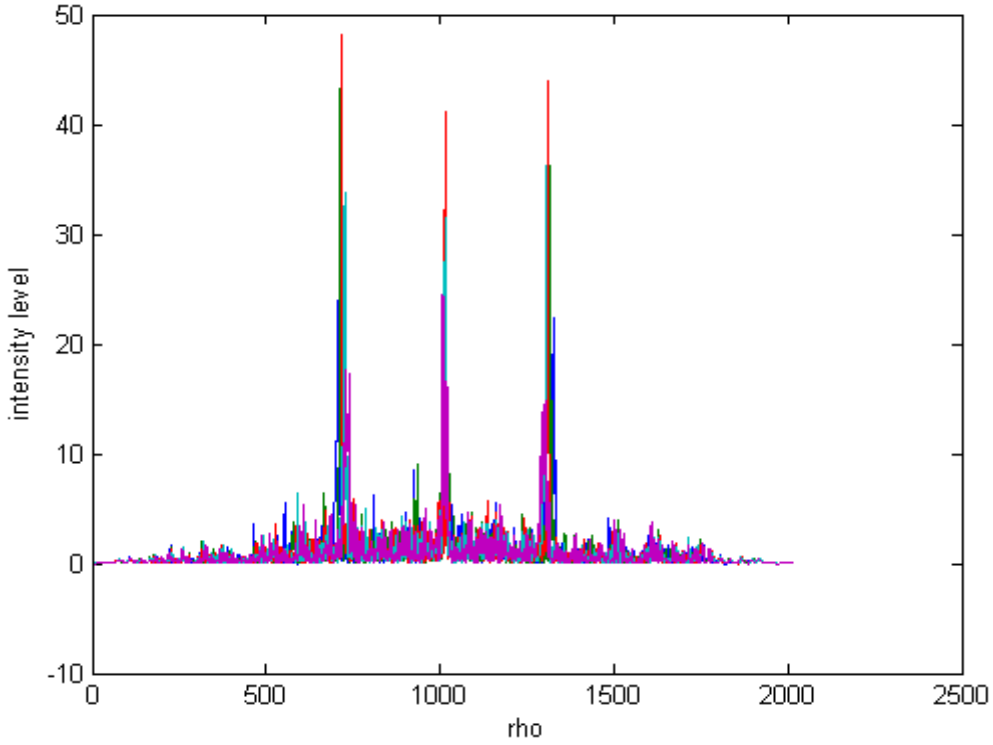


**Figure 4.9: Projection Vector at Angle $\theta_0$.**

The projection vector is thresholded with a threshold equal to one half of the maximum value of the projection vector. Figure 4.10 shows the thresholded projection vector.

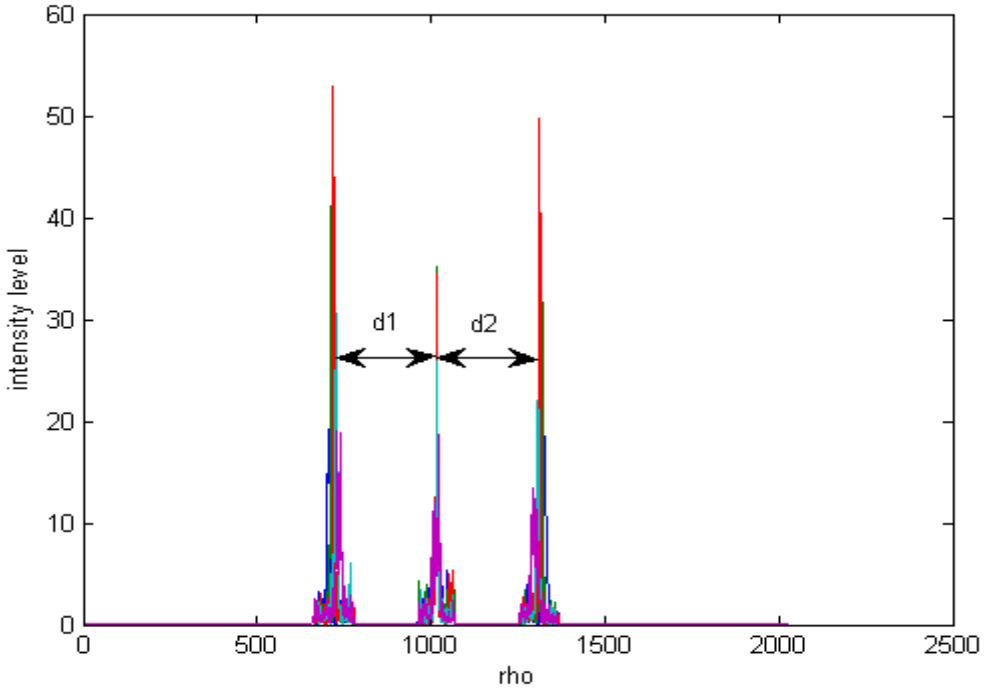


**Figure 4.10: Thresholded Projection Vector after Filtering.**

After thresholding, the distances can be found between the nonzero values in the projection vector which correspond to the consecutive modulation energy components. Several distances can be found between consecutive modulation energy components, and the final distance $d$ can be determined by finding the mean value of these distances. Recall from Figure 4.5, once $d$ is found the code period can also be found using the relation [18].

$$T = \frac{1}{F_s}\left(\frac{d}{\cos\theta_0}\right) \tag{4.4}$$

and the bandwidth can be found using the relation

$$B = \frac{\Delta f\left(\frac{d}{\cos\theta_0}\right)}{\tan\theta_0} \tag{4.5}$$

where $\Delta f$ is the frequency resolution of the PWVD image.

Once $F_c$, $T$ and $B$ are obtained the code length $N_c$ can be obtained using the relation $N_c = T \times B$ and the cycles of the carrier frequency per subcode $cpp$ can be obtained using the relation $cpp = {F_c}/{B}$.

## 4.3 PARAMETER EXTRACTION TEST RESULTS

The results of the parameter extraction algorithms are presented in Table 4.1. It shows the actual parameters used to generate the FM-CW signal. The simulation results showed that the algorithm proved well with low SNR levels of -6 dB. The error between the extracted parameter and the true value are relatively too small providing high accuracy rates in average. If $V_E$ is the extracted value of a signal whose true value is $V_T$, then the absolute value of the relative error $E_R$ is defined by [1]:

$$\mathrm{E_R} = \left|\frac{\mathrm{V_E} - \mathrm{V_T}}{\mathrm{V_T}}\right| = \left|\frac{Error}{True\ Value}\right|$$

The test results for FM-CW signals are presented below. The test results show that algorithm provide very good results and the algorithm have reasonably small errors. The carrier frequency error is very small for all SNR levels. Note that if the frequency resolution of the PWVD images are increased the carrier frequency error may decrease.

**Table 4.1. Parameter of test signal.**

| Signal | $F_c(Hz)$ | $B(Hz)$ | $T(s)$ |
|---|---|---|---|
| $F_1$ | 2000 | 1120 | 0.060 |
| $F_2$ | 1850 | 1380 | 0.040 |
| $F_3$ | 1280 | 720 | 0.080 |

The integration of the cross-term projection is very small as compared to the modulation projection for that the proposed algorithm is not affect from the cross-term present within the PWVD image.

**Table 4.2. Parameter extracted by Radon transform and Relative error rate.**

| Signal | SNR $(dB)$ | Extracted parameter | | | Error percentage | | |
|---|---|---|---|---|---|---|---|
| | | $F_c(Hz)$ | $B(Hz)$ | $T(s)$ | $F_c$-err | B-err | T-err |
| $F_1$ | 0 | 2001 | 1121 | 0.0603 | 0.50 | 0.089 | 0.5 |
| $F_2$ | 0 | 1853 | 1383 | 0.0401 | 0.16 | 0.21 | 0.25 |
| $F_3$ | 0 | 1283 | 723 | 0.0803 | 0.23 | 0.41 | 0.37 |
| $F_1$ | -3 | 2003 | 1123 | 0.0603 | 0.45 | 0.26 | 0.5 |
| $F_2$ | -3 | 1857 | 1387 | 0.0399 | 0.70 | 0.50 | 0.25 |
| $F_3$ | -3 | 1289 | 727 | 0.0796 | 0.70 | 0.97 | 0.5 |
| $F_1$ | -6 | 2014 | 1137 | 0.0604 | 1.05 | 1.51 | 0.66 |
| $F_2$ | -6 | 1859 | 1393 | 0.0403 | 1.08 | 0.94 | 0.87 |
| $F_3$ | -6 | 1291 | 736 | 0.0806 | 1.32 | 2.22 | 0.77 |

The parameter extraction test results for FM-CW Signal are presented for PWVD images in Table 4.2. The overall error rates are reasonably small. The carrier frequency error slightly increases from $SNR = 0dB$ to $SNR = -6dB$. The bandwidth and code period extraction results from PWVD images exhibit several high error rates for $SNR = -3dB$ and $SNR = -6dB$. This exhibits one of the drawbacks of the algorithm. As the $SNR$ level decrease below $0\,dB$ the maximum intensity level occurs at a very small projection angle $\theta_0$. This corresponds to the marginal time distribution and produce erroneous results.

# CHAPTER 5
# CONCLUSION AND FUTURE SCOPE OF WORK

## 5.1 CONCLUSION

In this dissertation FM-CW Signal detection is investigated. The architecture contained Time-frequency detection techniques which provide image outputs of FM-CW radar waveforms. The use of Time-frequency detection techniques provides an efficient method for the extraction of a composite feature vector to classify FM-CW Signals. An image cropping and feature extraction algorithm based on Radon Transform was applied to the Time-frequency images.

Concerning the test modulation results, the best overall classification result is achieved with PWVD technique. This might be due to the presence of the cross-terms within the PWVD images. Since cross-terms may preserve additional information about the modulation type, they might have improved the classification results.

Next the detection parameter extraction algorithms are investigated. Radon transform of the PWVD images was designed to extract the parameters from the PWVD images of FM-CW signals. The results obtained from algorithm tend to coincide well with the actual values and the relative error depends on how closely results are examined. At $SNR = -6dB$ the PWVD parameter extraction algorithm gave erroneous results.

## 5.2 FUTURE SCOPE OF WORK

The optimization process might be conducted in more detail. The use of bifrequency detection techniques may also be investigated for FM-CW waveform classification and parameter extraction.

Other feature extraction methods might be investigated such as Fisher Linear Discriminant Analysis which might improve the extraction of class discriminating information better. The information theoretic feature selection algorithms might also be investigated to select the best features from a potential feature set of a T-F image.

# PUBLICATIONS

1. Sudhir Kumar, “Parameter Estimation of Frequency Modulated Continuous Wave (FMCW) Radar Signal using Wigner-Ville Distribution and Radon Transform,” *International Journal of Advanced Research in Computer and Communication Engineering*, vol. 3, no. 6, pp. 6918-6921, 2014.

# REFERENCES


[1] P. E. Pace, "Detecting and Classifying Low Probability of Intercept Radar," Norwood, MA: Artech House, 2004.

[2] P. E. Pace and R. Cristi, "Extraction of Polyphase Radar Modulation Parameters using a Wigner-Ville Distribution Radon Transform," *IEEE International Conference on Acoustic, Speech and Signal Processing*, pp. 1505-1508, 2008.

[3] P. L. Shui, "Non-linear frequency modulated signal detection based on time-frequency tiling," *IEEE international Conference on Mobile and Wireless Communication*, vol. 2, pp. 409-412, 2004.

[4] A. Denk, "Detecting and Jamming Low Probability of Intercept (LPI) Radars," Master's Thesis, Naval Postgraduate School, Monterey, CA, 2006.

[5] D. L. Adamy, *EW102 A Second Course in Electronic Warfare*, Horizon House Publications, Inc., 2004.

[6] T. O Gulum, A. Y Erdogan and T. Yildirim, "Parameter Extraction of FMCW Modulated Radar Signals using Wigner-Hough Transform," *IEEE International Conference on Computational Intelligence and Informatics*, pp. 465-468, 2011.

[7] T. O. Gulum, "Autonomous Nonlinear Classification of LPI Radar Signal Modulations," Naval Postgraduate School Master's Thesis, 2007.

[8] H. V. Poor, *An Introduction to Signal Detection and Estimation*. Springer, 1998.

[9] H. Yousaf, F. Fahim and Z. Rasool, "FM-CW Radar Signal Processing Scheme," *Proceedings of International Bhurban Conference on Applied Sciences & Technology*, 2011.

[10] J. Yu-Gau, "Analysis of low probability of intercept radar signals using Wigner distribution," Chung-Cheng Institute of Technology Master's Thesis, 1992.

[11] E. R. Zilberman, "Autonomous Time-Frequency Cropping and Feature Extraction Algorithms for Classification of LPI Radar Modulations," Master's Thesis, Naval Postgraduate School, Monterey, CA, 2006.

[12] S. O. Piper, "Homodyne FMCW radar range resolution effects with sinusoidal nonlinearities in the frequency sweep," *Record of the IEEE International Radar Conference*, pp. 563-567, 1995.

[13] S. O. Piper, "Receiver frequency resolution for range resolution in homodyne FMCW radar," *Proceedings National Telesystems Conference, Commercial*

*Applications and Dual-Use Technology*, pp. 169-173, 1993.

[14] M. Edrich and H. Ziggler, "Ka-Band FMCW Radar for Sniper Detection," *IEEE International Radar Symposium*, pp. 201-204, 2012.

[15] P. L. Shui, "Non-linear Frequency Modulated Signal Detection Based on Time-frequency Tiling," *IEEE International Conference on Emerging Technologies: Frontiers of Mobile and Wireless Communication*, vol. 2, pp. 409-412, 2004.

[16] J. Fielding, "Polytime coding as a means of pulse compression," *IEEE Transactions on Aerospace and Electronic Systems*, vol. 35, no. 2, pp. 716-721, 1999.

[17] L. Cirillo, "Parameter Estimation for Locally Linear FM Signals Using a Time-Frequency Hough Transform," *IEEE Transactions on Signal Processing,* vol. 56, no. 9, pp. 4162-4175, 2008.

[18] T. O. Gulum, "Parameter Extraction Technique for FM-CW Radar Signals using Wigner-Hough Radon Transform," *IEEE International Conference on radar,* pp. 847-852, 2012.

[19] P. Hoogeboom, "Signal Processing Algorithms for FMCW Moving Target Indicator Synthetic Aperture Radar," *IEEE International Geoscience and Remote Sensing Symposium*, vol. 1, 2005.

[20] S. Mazuel and A. Huizing, "FMCW Radar System for Detection and Classification of Small Vessels in High Sea State Conditions," *IEEE International Conference on Microwave*, pp. 29-32, 2012.

[21] M. Brandt-Pearce, "Detection and Estimation of LFMCW Radar Signals," *IEEE Transactions on Aerospace and Electronic Systems*, vol. 48, no. 1, 2012.

[22] S. Kim, J. Lee, J. Park, D. Yeom and S. Park, "FPGA Based Signal Processing Module Design and Implementation for FMCW Vehicle Radar System," *IEEE International Conference on Robotics Research Division*, vol. 1, pp. 273-275, 2011.

[23] M. Mesbah and B. Boashash, "A Discrete time-frequency Wigner-Ville Distribution: Properties and Implementation," *Signal Processing Research Laboratory*, Brisbane, Australia, 2007.

[24] L. J. Spafford, "Optimum Radar Signal Processing in Clutter," *IEEE Transactions on Information Theory*, vol. 24, no. 5, pp. 734-743, 1968.

[25] L. G. Cuthbert and A.D. Olver, "Digital Signal Processing for Target in FMCW

Radar," *IEE Proceedings on Communications, Radar and Signal Processing*, vol. 128, no. 5, pp. 331-336, 1981.

[26] W. Yan, W. Shun and Y. Ming, "Implementation of Parallel Signal Processing System for All-Purpose Radar," *IEEE International conference on Signal Processing Proceeding*, vol. 2, pp. 1465-1468, 2002.

[27] L. Huan and L. Yubai, "A Practical FMCW Radar Signal Processing Method and Its System Implementation," *IEEE International Conference on ITS Telecommunication Proceedings*, pp. 1195-1199, 2006.

[28] C. Carlowitz, R. Wolf and F. Ellinger, "A Millimeter-Wave Low Power Active Back Scatter Tag for FMCW Radar System," *IEEE Transactions on Microwave Theory and Techniques*, vol. 61, no. 5, pp. 1964-1972, 2013.

[29] T. Long, "High-performance Universal Radar Signal Processing System," *IEEE International Conference on Signal Processing*, pp. 2254-2257, 2008.

[30] W. Daquan, "Signal Processing in the Life-Detection Radar Using an FMCW Waveform," *IEEE International Symposium on Information*, pp. 213-216, 2010.

[31] A. Zanalda, "A Combined Wigner-Ville and Hough Transform for Cross-Terms Suppression and Optimal Detection and Parameter Estimation," *IEEE International Conference on Acoustic, Speech and Signal Processing*, vol. 5, pp. 173-176, 1992.

[32] P. Luo, "A new method for estimating the number of targets from radar returns," *IEEE International Conference on Image and Signal Processing*, pp. 1-4, 2009.

[33] W. Tang and Y. Kuang, "A New Polynomial Phase Signal Detection Algorithm Based on the Combination of Filter Bank and Short-time Radon-Wigner Transform," *IEEE International Conference on Communication and Mobile Computing*, vol. 2, pp. 515-519, 2010.

[34] M. Lucian and R. Romulus, "Detection and Estimation of Linear FM Signals," *IEEE International Conference on Signals, Circuits and systems*, vol. 2, pp. 705-707, 2005.

[35] M. Gagilardo and M. Shao, "Application of Three Dimensional Filtering to Moving Target Detection," *IEEE Transactions on Aerospace and Electronic Systems*, vol. 19, no. 6, pp. 898-905, 1983.

[36] A. joubir and M. Amin, "Parameter Estimation for locally linear FM signals using a Time-Frequency Hough Transform," *IEEE International Conference on*

*Acoustic, Speech and Signal Processing*, vol. 3, pp. 3, 2006.

[37] Y. Jianyu, "LFM extended target echoes detecting using Radon-Wigner Method," *IEEE International Conference on Microwave and Millimeter Wave Technology*, pp. 1-4, 2007.

[38] H. Hang, "Time-Frequency DOA Estimation Based on Radon-Wigner Transform," *International Conference on Signal processing*, vol. 1, 2006.

[39] D. T. Barry, "Radon Transformation of Time-Frequency Distributions for Analysis of Multicomponent Signals," *IEEE International Conference on Acoustic, Speech and Signal Processing*, vol. 4, pp. 257-260, 1992.

[40] T. Farrel and G. Prescott, "Anine-tile algorithm for LPI signal detection using QMF filter bank trees," *IEEE Conference on Military Communication*, vol. 3, pp. 974-978, 1996

[41] F. Auger, P. Flandrin, P. Goncalves and O. Lemoine, *Time Frequency Toolbox*, CNRS, France, 1996.

[42] C. Gonzales, E. Woods and L. Eddins, Digital Image Processing Using Matlab, Upper Saddle River, NJ, Prentice Hall, 2004.

[43] P. Jarpa, "Quantifying the Differences in Low Probability of Intercept Radar Waveforms Using Quadrature Mirror Filtering," Master's Thesis, Naval Postgraduate School, Monterey, California, 2002.

[44] B. Lewis, F. Kretschmer and W. Shelton, *Aspects of Radar Signal Processing*, Artech House Inc., Norwood, MA, 1986.

[45] T. Kim and S. Choi, "Efficient radar target classification using adaptive joint time-frequency processing," *IEEE Transactions on Antennas and Propagation*, vol. 48, no. 12, pp. 1789-1801, 2000.

[46] M. R. Hejazi and G. Shevlyakov, "Modified Discrete Radon Transforms and Their Application to Rotation-Invariant Image Analysis," *IEEE Workshop on Multimedia Signal Processing*, pp. 429-434, 2006.

[47] S. Deans, *The radon transform and some of its applications*, John Wiley & Sons, Inc., New York, 1983.

[48] T. Claasen and W. Meckienbrauker, "Time-Frequency Signal Analysis by means of the Wigner Distribution," *IEEE International Conference on Acoustics, Speech and Signal Processing*, pp. 69-72, 1981.

[49] J. C. Cexus, A. O. Boudraa and A. Bouchikhi, "A combined Teager-Huang and

Hough Transform for LFM signal Detection," *IEEE International Symposium on Communications, Control and signal processing*, Limassoi, 2010.

[50] J. Marcum and P. Swerling, "Studies of Target Detection by Pulse Radar," *IRE Transactions on Information Theory*, vol. 6, no. 3, pp. 918-922, 1960

[51] S. Watts, "Radar Detection Prediction in K-Distributed Sea Clutter and Thermal Noise," *IEEE Transactions on Aerospace and Electronic Systems,* vol. 23, no. 1, pp. 40-45, 1987.

[52] X. Hou, N. Morinaga and T. Namekawa, "Direct Evaluation of Radar Detection Probabilities," *IEEE Transactions on Aerospace and Electronic Systems,* vol. 23, no. 4, pp. 418-424, 1985.

[53] X. Hou and N. Morinaga, "Detection Performance in K- Distributed and Correlated Rayleigh Clutter," *IEEE Transactions on Aerospace and Electronic Systems*, vol. 25, no. 5, 1989.

[54] G. L. Risueno and J. Grajal, "Atomic Decomposition-Based Radar Complex Signal Interception," *IEEE Transactions on Aerospace and Electronic Systems*, vol. 150, no. 4, pp. 323–331, 2003.

[55] G. L. Risueno and J. Grajal, "Multiple Signal Detection and Estimation Using Atomic Decomposition and EM," *IEEE Transactions on Aerospace and Electronic Systems*, vol. 42, no. 1, pp. 84–102, 2006.

[56] S. Barbarossa, "Analysis of Multicomponent LFM Signals by a Combined Wigner-Hough Transform," *IEEE Transactions on Signal Processing*, vol. 43, no. 6, pp. 1511–1515, 1995.

[57] B. W. Gillespie and L. E. Atlas, "Optimizing time-frequency kernels for classification," *IEEE Transactions on Signal Processing,* vol. 49, no. 3, pp. 485-496, 2001.

[58] Y. Barniv, "Dynamic Programming Solution for Detection Dim Moving Target," *IEEE Transactions on Aerospace and Electronic Systems,* vol. 21, no. 1, pp. 144-156, 1985.

[59] L. Cohen, "Time-Frequency distribution-A review," *Proceedings of the IEEE*, vol. 77, no. 7, pp. 941-981, 1989.

[60] D. K. Barton, "Simple Procedures for Radar Detection Calculations," *IEEE Transactions on Aerospace and Electronic Systems,* vol. 5, no. 5, pp. 837-846, 1969.

[61] J. Smith and R. Logan, "AN/APS-116 Periscope Detection Radar," *IEEE Transactions on Aerospace and Electronic Systems*, vol. 16, no. 1, pp. 66-73, 1980.

[62] *Image Processing Toolbox 5 User's Guide*, Natick, MA: The MathWorks, Inc., 2007

[63] B. D. Carlson, E. Evans and S. Wilson, "Search Radar Detection and Track with the Hough Transform," *IEEE Transactions on Aerospace and Electronic Systems*, vol. 30, no. 1, pp. 102-108, 1994.

[64] A. Nandi and E. Azzouz, "Algorithms for automatic modulation recognition of communication signals," *IEEE Transactions on Communications*, vol. 46, no. 4, pp. 431-436, 1998.

[65] S. Theodoridis, and K. Koutroumbas, *Pattern Recognition*, San Diego, CA: Academic Press, 2006.

[66] R. Frank, "Polyphase codes with good nonperiodic correlation properties," *IEEE Transactions on Information Theory*, vol. 9, no. 1, pp. 43-45, 1963

.